

UNIVERSITY OF TARTU
FACULTY OF SCIENCE AND TECHNOLOGY
Institute of Technology
Robotics and Computer Engineering

Ott Sellis

**INVESTIGATION AND COMPARISON OF KINETOSTATIC PERFORMANCE
INDICES FOR PARALLEL MECHANISMS**

Master's Thesis (30 ECTS)

Supervisors:

Assoc. Prof. Gholamreza Anbarjafari

Morteza Daneshmand

Tartu 2019

Abstract / Resümee

Investigation and Comparison of Kinetostatic Performance Indices for Parallel Mechanisms

For as long as we have used robots there has also been ongoing research to allow us to use and improve efficiency of automation in our daily lives. As our knowledge about robots has largely improved, so has the complexity of their structures. Thus, various methods and indices have been developed to help designers and engineers determine the best manipulator for a specific task. In addition, the interest towards parallel manipulators has seen growth in the last couple of years due to significantly better performance in various areas in comparison to serial mechanisms. However, no global performance index to evaluate accuracy and allow comparison in that perspective between parallel mechanisms has been developed. This thesis focuses on giving an overview on the developments towards finding a robust kinematic sensitivity index to measure accuracy performance of parallel manipulators.

Keywords: Parallel manipulator, kinetostatic performance indices

Paralleelmehhanismide kinetostaatiliste jõudlusindeksite uuring ning võrdlus

Nii kaua, kui on kasutusel olnud robotid, on käinud teadusuuringud nende kasutamiseks ning töö optimeerimiseks meie igapäevases elus. Samal ajal, kui meie teadmised robotite teemal on suuresti arenenud, on kasvanud ka vastavate struktuuride keerukus. Seega on arendatud mitmeid meetodeid ja indekseid, aitamaks disaineritel ning inseneridel välja selgitada parimad seadmed vastavate ülesannete lahendamiseks. Lisaks on huvi paralleelmehhanismide suunas viimaste aastate jooksul märgatavalt kasvanud. Peamiseks põhjuseks on paljudes valdkondades märgatavalt parem sooritusvõime võrreldes seriaalmanipulaatoritega. Ometi pole arendatud veel ühtegi globaalset jõudlusindeksit, mis võimaldaks täpsuse perspektiivis paralleelmanipulaatorite omavahelise võrdluse. Käesoleva lõputöö fookuseks on kintestaatilise jõudlusindeksi arendustööst ülevaate pakkumine. Uuritav indeks peab robustselt suutma hinnata läbi vastava indeksi paralleelmanipulaatorite täpsust.

Võtmesõnad: paralleelmanipulaatorid, kinetostaatilised jõudlusindeksid

CERCS: T125

Contents

Abstract / Resümee	1
Contents	2
List of Figures	4
List of Tables	6
Terms and Abbreviations	7
1 Introduction.....	8
2 Motivation.....	8
2.1 Serial vs Parallel manipulators	8
2.2 Kinetostatic performance indices	9
3 Literature review	9
3.1 Singularity Analysis of Closed-Loop kinematic Chains	9
3.2 Joint clearance	11
3.3 Jacobian, Manipulability, Condition Number, and Accuracy of Parallel Robots	12
3.3.1 Condition number	13
3.3.2 Isotropy and Global Conditioning Indices	14
3.4 Kinematic-Sensitivity Indices for Dimensionally Nonhomogeneous Jacobian Matrices.....	15
3.4.1 Indices for $q=\infty$	16
3.4.2 Proposed indices for $q = 2$	17
3.5 The Kinematic Sensitivity of Robotic Manipulators to Joint Clearances	18
3.5.1 Error on the Moving-Platform pose	19
3.5.2 Modelling clearances in an axisymmetrical joint	20
3.5.3 Computing the Maximum Moving-Platform Pose Errors	21

3.6	Geometric Analysis of the Kinematic Sensitivity of Planar Parallel Mechanisms ...	23
4	Recent work	27
4.1	Parameter sensitivity analysis of a 5-DoF parallel manipulator	27
4.1.1	Determination of variables and performance.....	29
4.1.2	Parameter definitions for substructure I.....	29
4.1.3	Parameter definitions for substructure II	30
4.1.4	Inverse Position Analysis.....	34
4.1.5	Stiffness modelling considering gravitational effects.....	37
4.1.6	Computing the stiffness model	42
4.1.7	The results.....	51
5	Analysis and comparison of indices	52
5.1	Future work	54
6	Summary.....	55
7	Kokkuvõte.....	56
8	Acknowledgements.....	57
8.1	58
9	References.....	58
10	Appendices.....	62
	Non-exclusive licence to reproduce thesis and make thesis public	71

List of Figures

Figure 1 – The 3-UPU robot [3]	11
Figure 2 – a) joint clearance between pin and hole of i^{th} and j^{th} link accordingly. b) equivalent clearance link r [6].	11
Figure 3 – The motion cycle of a four-bar linkage. Small and big dotted lines having the clearance of 0.01 and 0.02 accordingly [6].	12
Figure 4 – Mapping between the joint errors space and the generalized error space. Euclidian norm on top and infinity norm on the bottom. Using these norms, the relation between joint errors $\Delta\theta_1$ and $\Delta\theta_2$ is illustrated [3].	13
Figure 5 – $(\mathbf{P}_6(\mathbf{K}))$ indicates the envelope of the displacement's zonotope. $(\mathbf{P}_6(\mathbf{T}(t)))$ is the right prism where the surrounding hyperplanes consist of symmetric pairs with respect to the origin. (The parentheses show that the illustration is an analogy in a lower-dimensional space) [22].	16
Figure 6 – Analogy of mapping the six-dimensional ellipsoid into \mathbb{R}^3 . Using rotational displacement as an example. $\mathbf{E} = \mathbf{KpTPrKp}$ and \mathbf{K} being the inverse Jacobian matrix. \mathbf{H} denotes the transformation matrix [22].	17
Figure 7 – Geometrical representation of the variations of kinematic sensitivity in the case of a constrained manipulator [25].	25
Figure 8 – Geometric representation of the kinematic sensitivity constraints for a 3-RPR parallel manipulator with a locked actuator [25].	26
Figure 9 – T5 PM and its Subsystems [26].	29
Figure 10 – Structure and parameters of Subsystem I [26]	30
Figure 11 – Structure and parameters of subsystem II [26].	31
Figure 12 – (a) 3-D model and (b) schematic diagram of T5 PM [28].	35
Figure 13 – (a) Description of platform I and (b) schematic diagram of substructure II [28].	36
Figure 14 – Free-body diagrams of substructure I (a) and substructure II (b) [28]	38
Figure 15 – Force and deformation of IR_1 and IR_2 [28].	42
Figure 16 – Components of the P-joint in the UPS limb [27].	44
Figure 17 – 3-D model of S joint in the 1 st , 2 nd , 3 rd , and 4 th UPS limb [28].	45
Figure 18 – Free body diagram of the UP limb [28].	47
Figure 19 – 3-D model of closed-loop I (left) and II (right) [28]	49

Figure 20 – Proportions of parameter impacts to performance reliability of subsystem I (green: 1st to 4th UPS limbs, yellow: IR joints, blue: UP limb, pink: 5th UPS limb, red numbers indicating corresponding reliability sensitivity to parameter mean values) [26].....69

Figure 21 – Proportions of parameter impacts to performance reliability of subsystem II (green: 1st to 4th UPS limbs, yellow: IR joints, blue: UP limb, pink: 5th UPS limb red numbers indicating corresponding reliability sensitivity to parameter mean values) [26].....70

List of Tables

Table 1 – Configuration of the measuring point in frame O-xyz [28]	34
Table 2 – Accuracy assessment of response models for subsystem I [26].	62
Table 3 – Accuracy assessment of response models for subsystem II [26].	63
Table 4 – Dimensional parameters and workspace of T5 PKM [28].....	64
Table 5 – Lead screw parameters and compliance of R joints [28]	64
Table 6 – Compliance coefficients of UPS limbs (unit: $(\mu\text{m}/\text{N}) \times 10^{-3}$) [28].....	64
Table 7 – Lead screw parameters and compliance of R joints [28]	64
Table 8 – Compliance coefficients of UP limb [28]	64
Table 9 – Component compliance coefficients of closed-loop I in substructure II[28].....	65
Table 10 – Component compliance coefficients of closed-loop II in substructure II[28]	65
Table 11 – Mass and centre of mass of components in substructure I[28]	65
Table 12 – Mass and centre of mass of components in substructure II [28][28]	66
Table 13 – Global parameter sensitivity of performance reliability in subsystem I [26].....	67
Table 14 – Global parameter sensitivity of performance reliability in subsystem II [26]	68

Terms and Abbreviations

DOF – Degree of Freedom

PM – Parallel Manipulator

OP – Operating point.

S – actuated spherical joint

R – actuated rotational joint

P – actuated prismatic joint

FFD – Full Factorial Design

CCD – Central Composite Design

BBD – Box-Behnken Design

LHD – Latin Hypercube Design

RSAV – Reliability Sensitivity Absolute Value

RSPC – Reliability Sensitivity Positive Correlation

RSNC – Reliability Sensitivity Negative Correlation

NSGA-II – Non-dominated Sorting Genetic Algorithm II

FEA – Finite element Analysis

AI – Artificial Intelligence

1 Introduction

In this thesis, an investigation and comparison of kinetostatic performance indices for parallel manipulators is carried out. Indices are described in detail and their experimental results are provided. In addition, a comparative analysis between the performance indices is provided for the engineers to be able to choose which type of indices to focus on. Lastly, an insight on a more recent work on the topic of kinetostatic performance indices is presented to show how what has improved and what problems have remained.

2 Motivation

Robots have been a major part in the industry for a while now and the rapid growth of robotics does not seem to stop on the near future. On the contrary, robot manipulators are being introduced to new fields on a regular basis. The stamina, durability, power and robustness of robots have made them the main workforce in factories for example, substituting manual labour in most mainstream industries [1].

2.1 Serial vs Parallel manipulators

The industrial robots, also known as manipulators, can be categorized into two types based on their build: serial and parallel. A parallel manipulator can be defined as a closed loop kinematic chain mechanism whose end effector is linked to the base by several independent kinematic chains as opposed to a serial manipulator, which is linked by only one chain [2]. Parallel manipulators are gaining popularity recently, although various drawbacks in comparison to the serial versions can be noticed like smaller workspace, lower dexterity and considerably more complex kinematic calculations. These negative properties can be overlooked in applications, which require high accuracy or high loading capabilities as the complex closed loop build of parallel manipulators increase the performance in aforementioned areas. Greater load capacity is achieved due to the shared load of parallel links connected to the fixed base. The use of multi degree of freedom spherical and universal joints in PMs makes sure that the legs experience only compressive or tensile loads, but no shear forces or bending and torsion moments. This in fact not only increases load capacity but also reduces deformation of the platform under high load forces thus making it more precise. The parallel robot designs all have actuators within or

near the base, which guarantees a higher bandwidth with low inertia. This is why PMs are used for example in flight simulators, fast pick and place robots, precision surgery or complex welding.

2.2 Kinetostatic performance indices

Kinetostatic indices, opposed to dynamic performance indices, which focus on the movement path of the end-effector from one pose to another, are used to analyse the accuracy of a manipulator reaching a certain pose. Since serial manipulators have been used in the industry much longer than their parallel counterparts have, they have been more thoroughly researched. Thus, various indices to differentiate one from another have been developed over the years to suit the growing demands of designers in all areas of robotics. Research has shown that indices suitable for serial manipulators do not apply to parallel manipulators as their more complex build either negate the distinctiveness of the indices or in worse cases make them impossible to compute [3]. An overview of the indices as well as an analysis is presented in the following sections. It must be noted that once a joint, spherical joint (S) for example, is underlined, it defines it as actuated, while joints without underlining are considered passive.

3 Literature review

In this paragraph, a short summary of literature considering kinetostatic performance indices of parallel manipulators is presented. In addition, the history and background is discussed and a brief analysis of the indices discussed is presented in paragraph 5.

3.1 Singularity Analysis of Closed-Loop kinematic Chains

The study of kinematic chains leads inevitably to the problem of singular configurations in which the Jacobian matrices become rank deficient. These matrices are used to describe transformation from one frame to another. For this case, the Jacobian from the origin to the end-effector frame is considered. In other words, the degree of freedom of the system changes instantaneously [4]. Since the time Angeles' article was released, there was very little research done on the singularity problem of closed-loop kinematic chains. So a general classification, which would include both singular and parallel types of mechanisms, is proposed. These

singularities are sorted into 3 types. The first describing the situation where the end-effector of an operator reaches the boundary of its workspace, removing all degrees of freedom pointing outward. The second variation occurs when all actuated joints are locked or immobile, but the end-effector still has forces or moments about an axis. Lastly, the third type being both singularities taking place simultaneously. The author shows that these phenomena can be described in two equations:

$$\det(\mathbf{A}) = 0, \det(\mathbf{B}) = 0 \quad (1)$$

where

$$\mathbf{A} = \frac{\partial \mathbf{F}}{\partial \mathbf{x}}, \mathbf{B} = \frac{\partial \mathbf{F}}{\partial \theta} \quad (2)$$

θ and x denote the output and input coordinates accordingly whilst \mathbf{F} represents the relation between the two. As mentioned before, \mathbf{A} and \mathbf{B} are both Jacobian matrices which indicates that to find the singularities one must solve the inverse or forward kinematic problem. It is shown via multiple robotic systems that solving either problem becomes more difficult as the degrees of freedom and the complexity of the structure increases especially when dealing with parallel manipulators.

In a more recent work by Merlet [3] the Jacobian matrices are extended to not only describing the actuated joints but also including passive joints and their interactions. The number of passive joints in parallel manipulators being usually significantly larger than their linear counterparts are. Merlet postulates that systems with less than 6 controllable degree of freedom (DOF) should have their end effector be considered as a 6 DOF rigid body. This indicates that positioning errors must be examined for all degrees, adding singularities like unmeasured motion of active joints, which can also be attributed to joint clearance or increased instantaneous mobility. A practical example of a 3-UPU, see Figure 1, robot is used to exemplify the additional singularities. It was discovered that when all legs had identical length and the prismatic actuators were locked, the end-effector was having significant orientation motion. Since the determinant of the inverse kinematic Jacobian did not equal 0 in any of the poses it meant that it was not a singular pose as described by Angeles [4]. The first to explain this phenomenon were Bonev and Zlatanov [5] who described it as constraint singularity. They used Plücker vectors to describe a 3 DOF manipulator as 6 DOF. By doing so, they also proved that accuracy analysis cannot be decoupled from singularity analysis. In addition, it is always necessary to consider the full inverse kinematic Jacobian whilst carrying out the analysis.

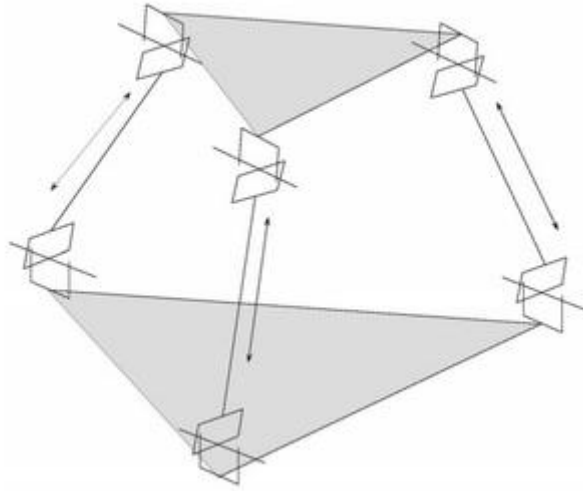


Figure 1 – The 3-UPU robot [3]

3.2 Joint clearance

In the article by Tsai and Lai [6] the term joint clearances in the linkages of mechanisms is explained and elaborated as well as the concept of a reciprocal screw to constrain the movements of joints, to evaluate the effect of joint clearances on transmission performance. The usage of a screw enables finding the actual output error, which is critical in precision machine design. Joint clearance is defined as unwanted movement within a linkage of a machine and is described via a virtual link.

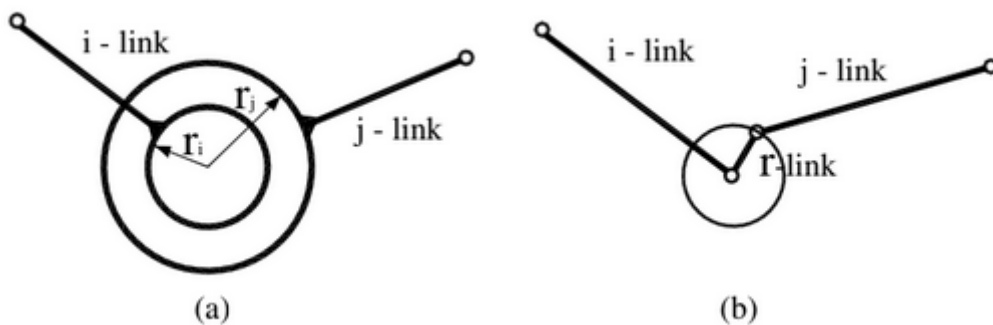


Figure 2 – a) joint clearance between pin and hole of i^{th} and j^{th} link accordingly. b) equivalent clearance link r [6].

The four-bar linkage motion cycle, illustrated on Figure 3, is used to imply numerical solutions and test this theory. One can see that the difference between an ideal joint and one having

clearance is highest near the dead-center position. As the clearance value drops, so does the difference thus confirming the direct effect, albeit small, this measure has on the accuracy performance of a mechanism.

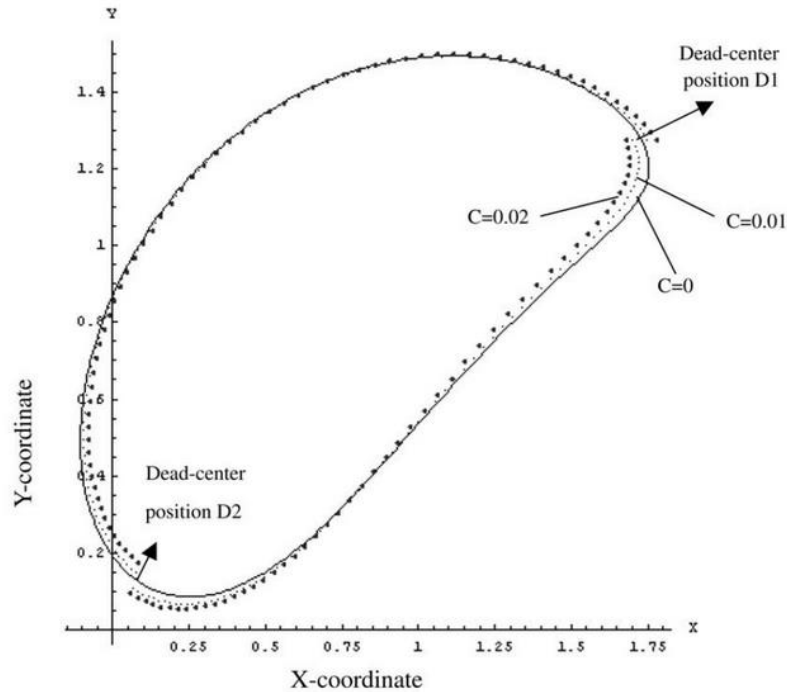


Figure 3 – The motion cycle of a four-bar linkage. Small and big dotted lines having the clearance of 0.01 and 0.02 accordingly [6].

3.3 Jacobian, Manipulability, Condition Number, and Accuracy of Parallel Robots

In the aforementioned paper by Merlet [3], multiple indices are discussed. Starting with manipulability which is a classical concept that describes the dexterity of a robot. It models the velocity amplification of each joint via two types of norms. One being the Euclidian norm which geometrically produces a circle that turns into an ellipsoid when ran through the Jacobian matrix. The closer the geometry is to a circle the better. The other, infinity norm, plots the results as a square or rectangle accordingly.

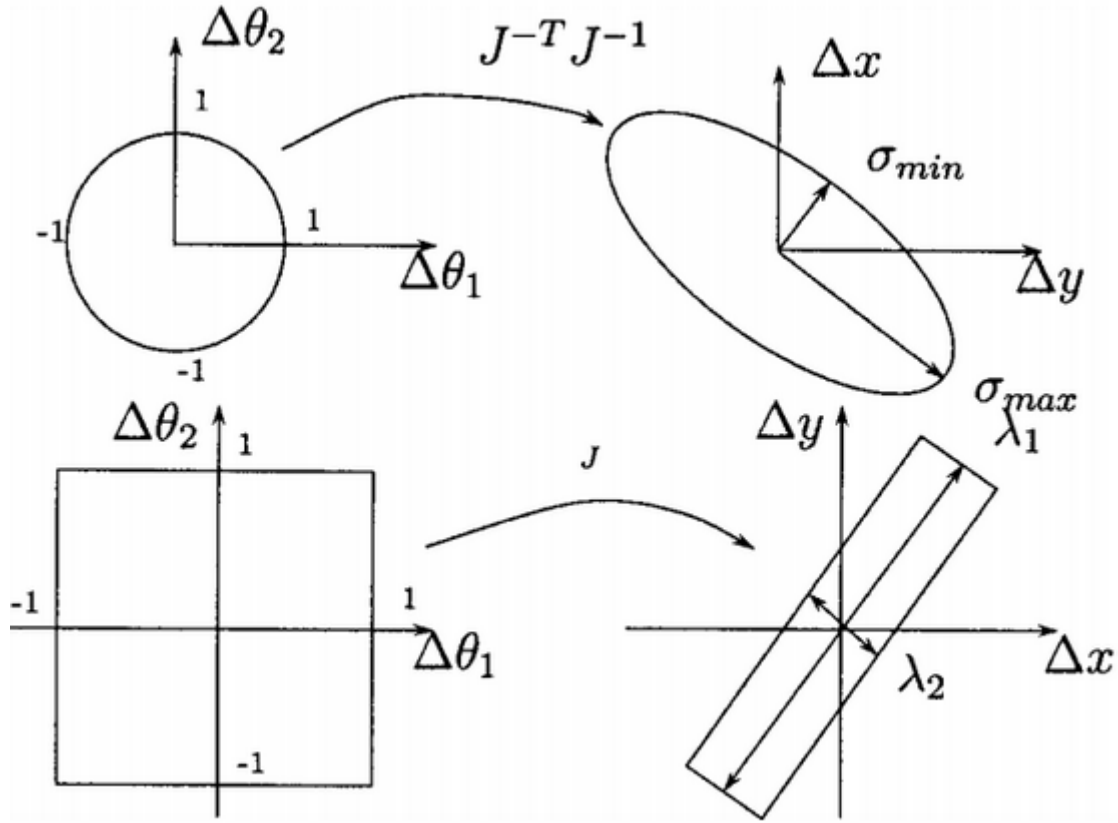


Figure 4 – Mapping between the joint errors space and the generalized error space. Euclidian norm on top and infinity norm on the bottom. Using these norms, the relation between joint errors $\Delta\theta_1$ and $\Delta\theta_2$ is illustrated [3].

Staffetti et al. [7] stated that the use of Euclidian norm is not realistic due to the fact that if one of the errors is 1, all other joint errors become exactly 0. The infinity norm overcomes this, by bounding each joint error independently by 1. It also covers the Euclidian norm ellipsoid so no loss of information occurs. In addition, the rectangular shape is mathematically easy to manipulate. The biggest drawback of manipulability is that it can only view translation and rotation separately, since there is no differentiation of units, thus amplification involving motions within both fields cannot be directly estimated.

3.3.1 Condition number

Whilst a large dimension along an axis of the manipulability polyhedron indicates a large amplification, it does not quantify the error. Therefore, an index called condition number is used to solve the problem. The condition number κ is defined as:

$$\kappa(J) = \kappa(J^{-1}) = \|J^{-1}\| \|J\| \quad (3)$$

With J being the inverse kinematic Jacobian matrix. It is visible that the condition number is dependent on the choice of matrix norm. The two-norm and the Euclidean norm being the most used variations. First of which defined as the square root of the largest eigenvalue of matrix $J^T J^{-1}$, where condition number is the ratio between the smallest and largest eigenvalue of $J^T J^{-1}$. For the Euclidean it is the ratio between $\sum \lambda_i^2$ and $\prod \lambda_i$, where λ is the eigenvalue.

The condition number can be used to determine various attributes:

- the accuracy/dexterity of a robot [8, 9, 10]
- the closeness of a pose to singularity [11] Although in general it is impossible to define a mathematical distance where DOF contain both translation and orientation.
- performance criteria for optimal design and comparison of robots [12, 13, 14, 15, 16, 17, 18, 19, 20]
- the useful workspace of a robot [13]

Despite these functionalities, the condition number has one major drawback. Similar to the manipulability index, the matrix involved in its calculation is not homogeneous in terms of units. Hence, the value of the number changes between translational and orientational DOF although the kinematic accuracy is constant. There exists a workaround via a normalized inverse Jacobian matrix, but it is difficult to use with complex geometry and is overall not an intuitive method for measuring accuracy. End users are more likely interested in maximal positioning error rather than relative value which the condition number offers. Thus, the use of condition number, although possible for determining maximal positioning errors has to be carefully considered.

3.3.2 Isotropy and Global Conditioning Indices

An isotropic pose of a robot is defined as a pose where the condition number κ is equal to 1. A parallel robot having isotropic poses in its workspace is often considered as a design objective. Merlet [3] notes that this objective holds no true value in terms of accuracy assessment as using a serial Cartesian X-Y robot for example whose kinematic Jacobian Matrix is the identity matrix the results for maximal velocity alternate within the range $[1, \sqrt{2}]$. Since the X-Y robot has a very simple build and already has problems in this field one can easily determine that using isotropy for positioning error analysis holds no merit.

The global conditioning index, which was proposed by C. Gosselin [21] is used to evaluate the dexterity of a robot over a given workspace. This is done via averaging the condition number over said workspace. Although the aforementioned index solves the problem of locality for κ . It still contains the same validity problems discussed in section 3.3.1. In addition, the robust calculation of the index suggests that obtaining the results is computationally very heavy. This leads to sampling which causes additional problems, mainly involving the smoothness evaluation of the condition number to validate the probing method.

Overall as seen from the work by Merlet [3], classical dexterity indices are not ideal to assess accuracy for parallel robots. All of which come with some form of drawbacks whose significance increases with the complexity of the build of the mechanism in question. As parallel mechanisms typically have more complex structure in comparison to serial mechanisms, using said indices as they are raise many questions regarding the validity of accuracy assessment.

3.4 Kinematic-Sensitivity Indices for Dimensionally Nonhomogeneous Jacobian Matrices

The paper from P. Cardou et al. [22] discusses the matter of accuracy assessment for systems with a Nonhomogeneous Jacobian Matrix. For clarification, the indices mentioned previously are only applicable to homogeneous matrices. It is also stated that the research only covers local performance indices, meaning that only given postures are examined as opposed to the whole workspace. The authors also give some constraints to their proposed indices:

- No dependencies on the end-effector geometry, since it makes comparison between multiple manipulators difficult.
- The Jacobian Matrices in question will not be normalized because the selection of values used in the process will sidetrack the accuracy assessment.

An experiment is conducted for finding the compatible actuator displacements θ , which have unit in p -norm, which the author renames q -norm due to the fact that the p is used as a subscript for translational movements. Displacements are regarded compatible if and only if they can produce a pose for an end effector rigidly i.e. when $q = 1$ where q denotes the aforementioned q -norm unit. This leads to two possible definitions for the indices. The maximum-magnitude rotation and point displacement under a unit-norm displacement, which can be shown as:

$$\sigma_{r,q} \equiv \max_{\|\theta\|_q=1} \|\phi\|_q \quad (4)$$

$$\sigma_{p,q} \equiv \max_{\|\theta\|_q=1} \|p\|_q \quad (5)$$

where ϕ and p are rotational and translational displacements accordingly.

3.4.1 Indices for $q=\infty$.

Using the infinity norm leads to all of the points being contained in a hypercube centred at the origin and having two dimensional edges.

For serial manipulators computing the infinity norm of a matrix merely comes down to choosing the greatest of the one norms of its row vectors.

For parallel manipulators, it is more complicated. As by the time this article was released no explicit symbolical solution had been found. To solve this, Cardou et al. [22] used a geometrical constraint to form an envelope of a zonotope in \mathbb{R}^6 , which describes the displacements' matrix. It works the same for both the rotation and translation sensitivity. Using the infinity norm deducts to forming an envelope of a right prism with a square cross-section and infinite length around the zonotope so that it contains every value of $\sigma_{r,q}$ or $\sigma_{p,q}$. Figure 5 is used to illustrate this method.

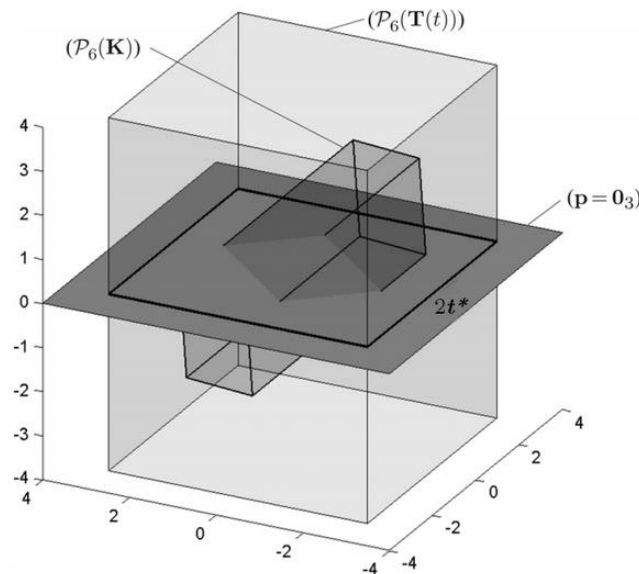


Figure 5 – $(P_6(\mathbf{K}))$ indicates the envelope of the displacement's zonotope. $(P_6(\mathbf{T}(t)))$ is the right prism where the surrounding hyperplanes consist of symmetric pairs with respect to the origin. (The parentheses show that the illustration is an analogy in a lower-dimensional space) [22].

When choosing between supporting hyperplanes the farthest from origin is always taken since we are looking for maximal displacement errors, namely:

$$\sigma_{r,\infty} = \max_{i=1,2,3} \left(\max_x e_i^T x, \quad s. t. \mathbf{L}x - \mathbf{1}_{2n} \leq 0_{2n} \right) \quad (6)$$

$$\sigma_{p,\infty} = \max_{i=4,5,6} \left(\max_z e_i^T z, \quad s. t. \mathbf{L}x - \mathbf{1}_{2n} \leq 0_{2n} \right) \quad (7)$$

where e_i is the normal vector of $\mathbf{P}_6(\mathbf{K})$ and \mathbf{L} denotes the component-wise inequality of \mathbf{K} .

3.4.2 Proposed indices for $q = 2$

Although the infinity-norm offers a sound physical interpretation Cardou et.al. [22] state that it does not allow a closed-form solution for parallel manipulators. Thus the 2-norm is used and whilst it has no physical interpretation as actuated-joint displacements are taken to be independent. In their paper it is regarded as the approximation of the ∞ -norm as it is bounded by the 2-norm from both sides. Thus the transformation is regarded as approximating a box around the hypersphere of the ∞ -norm.

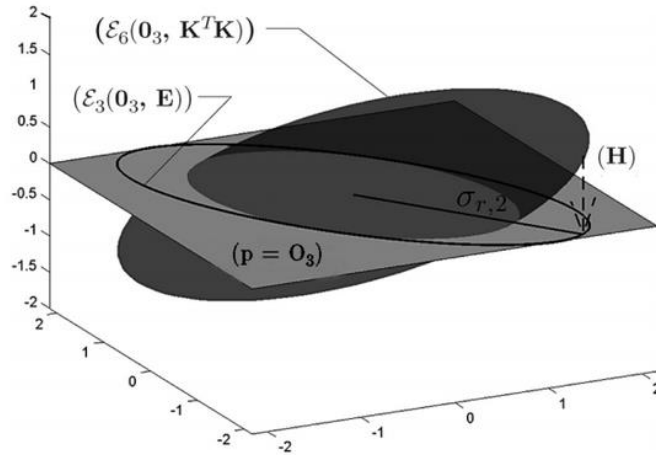


Figure 6 – Analogy of mapping the six-dimensional ellipsoid into \mathbb{R}^3 . Using rotational displacement as an example. $\mathbf{E} = \mathbf{K}_p^T \mathbf{P}_r \mathbf{K}_p$ and \mathbf{K} being the inverse Jacobian matrix. \mathbf{H} denotes the transformation matrix [22].

The computations for rotational and translational displacements of parallel manipulators are again identical. Contrary to the ∞ -norm, the constraint equation geometrically forms an ellipsoid similar to the manipulability index mentioned in the beginning of section 3.3. Working on the ellipsoid is mathematically more complex as projecting a six-dimensional ellipsoid onto a 3-D subspace requires a special case of ellipsoid propagation, defined by Ros et al. [23]. Overall, the maximal displacements can be calculated as follows:

$$\sigma_{r,2} = \frac{1}{\sqrt{\min_{i=1,2,3} \lambda_{rp,i}}} = \sqrt{\|(K_r^T P_p K_r)\|_2} \quad (8)$$

where $P_p \equiv \mathbf{1}_{6 \times 6} - K_p (K_p^T K_p)^{-1} K_p^T$ is the projection matrix onto the left nullspace of K_p and $K_p = KH^\perp$ with $H^\perp \equiv [\mathbf{0}_{3 \times 3} \quad \mathbf{1}_{3 \times 3}]^T$ which is illustrated on Figure 6. $\lambda_{rp,i}$ are the eigenvalues of $K_r^T P_p K_r$.

$$\sigma_{p,2} = \frac{1}{\sqrt{\min_{i=1,2,3} \lambda_{pr,i}}} = \sqrt{\|(K_p^T P_r K_p)\|_2} \quad (9)$$

where $P_r \equiv \mathbf{1}_{n \times n} - K_r (K_r^T K_r)^{-1} K_r^T$ and $K_r = KH^T$ and $H^T \equiv [\mathbf{1}_{3 \times 3} \quad \mathbf{0}_{3 \times 3}]^T$.

The indices proposed in this section solve some problems previous indices are not able to mainly:

- 1) Giving measures to maximum displacements with clear physical meaning.
- 2) They rely on the Jacobian alone, thus the choice of points outside of operating point is impossible.
- 3) Dependence on the choice of OP
- 4) Compliance with any uniformly actuated manipulator – redundantly actuated or not.

Still, if it is required that the manipulator is uniformly actuated, the applicability of the indices proposed in this section comes to question.

3.5 The Kinematic Sensitivity of Robotic Manipulators to Joint Clearances

In this paper by Binaud et al. [24] Denavit-Hartenberg parameters are used to parameterize the manipulators. This yields to each joint having its own reference frame each of which is related to the previous one via a screw:

$$\mathbf{S}_{i,j} = \begin{bmatrix} \mathbf{R}_{i,j} & \mathbf{t}_{i,j} \\ \mathbf{0}_3^T & 1 \end{bmatrix} \in SE(3) \quad (10)$$

where $\mathbf{R}_{i,j}$ is a 3x3 rotation matrix, \mathbf{t} points from the frame in question to the next frame and $\mathbf{0}_3$ is the three-dimensional zero vector. Since the frames follow Denavit-Hartenberg convention $\mathbf{S}_{i,j}$ can be expressed as

$$\mathbf{S}_{i,j} = \mathbf{S}_{i,j,\theta} \mathbf{S}_{i,j,b} \mathbf{S}_{i,j,a} \mathbf{S}_{i,j,\alpha} \quad (11)$$

where

$$\mathbf{S}_{i,j,\alpha} = \begin{bmatrix} 1 & 0 & 0 & 0 \\ 0 & \cos \alpha_{i,j} & \sin \alpha_{i,j} & 0 \\ 0 & -\sin \alpha_{i,j} & \cos \alpha_{i,j} & 0 \\ 0 & 0 & 0 & 1 \end{bmatrix} \quad (12)$$

$$\mathbf{S}_{i,j,a} = \begin{bmatrix} 1 & 0 & 0 & a_{i,j} \\ 0 & 1 & 0 & 0 \\ 0 & 0 & 1 & 0 \\ 0 & 0 & 0 & 1 \end{bmatrix} \quad (13)$$

$$\mathbf{S}_{i,j,b} = \begin{bmatrix} 1 & 0 & 0 & 0 \\ 0 & 1 & 0 & 0 \\ 0 & 0 & 1 & b_{i,j} \\ 0 & 0 & 0 & 1 \end{bmatrix} \quad (14)$$

$$\mathbf{S}_{i,j,\theta} = \begin{bmatrix} \cos \theta_{i,j} & \sin \theta_{i,j} & 0 & 0 \\ -\sin \theta_{i,j} & \cos \theta_{i,j} & 0 & 0 \\ 0 & 0 & 1 & 0 \\ 0 & 0 & 0 & 1 \end{bmatrix} \quad (15)$$

and where $\alpha_{i,j}, a_{i,j}, b_{i,j}, \theta_{i,j}$ represent link twist, link length, link offset and joint angle accordingly. For revolute joints $\theta_{i,j}$ is the variable, as opposed to prismatic joints where $b_{i,j}$ is the variable. Hence, the pose of the sixth link from the i^{th} frame can be expressed as the product of screws from said frame.

3.5.1 Error on the Moving-Platform pose

The joint-clearance errors can be expressed by a screw as well via a vector or a 4x4 matrix

$$\delta \mathbf{s}_{i,j} \equiv \begin{bmatrix} \delta \mathbf{r}_{i,j} \\ \delta \mathbf{t}_{i,j} \end{bmatrix}, \quad \delta \mathbf{S}_{i,j} = \begin{bmatrix} \delta \mathbf{R}_{i,j} & \delta \mathbf{t}_{i,j} \\ \mathbf{0}_3^T & 1 \end{bmatrix} \in se(3) \quad (16)$$

where $\delta \mathbf{R}_{i,j} \equiv \partial(\delta \mathbf{r}_{i,j} \times \mathbf{x})/\partial \mathbf{x}$ is the cross product matrix of $\delta \mathbf{r}_{i,j}$. Because of joint clearances the calculation for the i^{th} link pose also changes to

$$\mathbf{P}'_i = \prod_{j=1}^{n_i} \mathbf{e}^{\delta \mathbf{S}_{i,j}} \mathbf{S}_{i,j} \quad (17)$$

where $\mathbf{e}^{\delta \mathbf{S}_{i,j}}$ is the matrix exponential of $\delta \mathbf{S}_{i,j}$ and adds displacement to the i^{th} frame. \mathbf{P}'_i takes the i^{th} frame of the j^{th} limb to its pose on the moving platform frame. In order to compute the moving-platform pose error a new screw of $\Delta \mathbf{P}_{i|\mathcal{P}'_i}$ is introduced. It takes the nominal moving-platform pose \mathcal{P}_i on to the shifted \mathcal{P}'_i through the i^{th} leg and is expressed in frame \mathcal{P}_i as

$$\delta \mathbf{P}_{i|\mathcal{P}_i} = \sum_{j=1}^{n_i} \left(\prod_{k=n_i}^j \mathbf{S}_{i,k}^{-1} \delta \mathbf{S}_{i,j} \prod_{l=j}^{n_i} \mathbf{S}_{i,l} \right) \quad (18)$$

which can alternatively be computed as a vector $\delta \mathbf{p}_{i|\mathcal{P}_i}$

$$\delta \mathbf{p}_{i|\mathcal{P}_i} \equiv \sum_{j=1}^{n_i} \prod_{k=n_i}^j \left(\text{adj}(\mathbf{S}_{i,k}) \right)^{-1} \delta \mathbf{s}_{i,j} \quad (19)$$

where

$$\text{adj}(\mathbf{S}_{i,j}) \equiv \begin{bmatrix} \mathbf{R}_{i,j} & \mathbf{O}_{3 \times 3} \\ \mathbf{T}_{i,j} \mathbf{R}_{i,j} & \mathbf{R}_{i,j} \end{bmatrix} \quad (20)$$

with $\mathbf{T}_{i,j}$ being the cross-product matrix of $\mathbf{t}_{i,j}$.

$$\mathbf{T}_{i,j} \equiv \delta(\mathbf{t}_{i,j} \times \mathbf{x}) / \delta \mathbf{x} \quad (21)$$

In this manner, $\delta \mathbf{p}_{i|\mathcal{P}_i}$ is expressed in frame \mathcal{P}_i . To show this small displacement screw in frame 1 of the i^{th} leg:

$$\delta \mathbf{p}_{i|F_{i,1}} = \prod_{j=1}^{n_i} (\mathbf{N}_{i,j}) \delta \mathbf{p}_{i|\mathcal{P}_i} \quad (22)$$

where

$$\mathbf{N}_{i,j} \equiv \begin{bmatrix} \mathbf{R}_{i,j} & \mathbf{O}_{3 \times 3} \\ \mathbf{O}_{3 \times 3} & \mathbf{R}_{i,j} \end{bmatrix} \quad (23)$$

As a result, we get this compact form:

$$\delta \mathbf{p}_{i|F_{i,1}} = \mathbf{M}_i \delta \mathbf{s}_i \quad (24)$$

where

$$\mathbf{M}_i \equiv [\mathbf{M}_{i,1} \quad \mathbf{M}_{i,2} \quad \cdots \quad \mathbf{M}_{i,n_i}], \quad (25)$$

$$\mathbf{M}_{i,j} \equiv \prod_{l=1}^{n_i} (\mathbf{N}_{i,l}) \prod_{k=n_i}^j \left(\text{adj}(\mathbf{S}_{i,k}) \right)^{-1} \quad (26)$$

$$\delta \mathbf{s}_i \equiv [\delta \mathbf{s}_{i,1}^T \quad \delta \mathbf{s}_{i,2}^T \quad \cdots \quad \delta \mathbf{s}_{i,n_i}^T]^T \quad (27)$$

3.5.2 Modelling clearances in an axisymmetrical joint

When modelling clearances, usually associated errors are bound. This yields to six parameters if both lower and upper bounds are the same, unless the joints are considered axisymmetric. In

this case, according to the Denavit-Hartenberg convention, the Z-axis is aligned with the revolute-joint axis. In addition, if the origin of the j^{th} joint of the i^{th} leg's frame is chosen to lie at the centroid of the revolute joint, the Z components of $\delta \mathbf{r}_{i,j}$ and $\delta \mathbf{t}_{i,j}$ are axial whilst X and Y components remain radial. Thus, the error bounds can be written as

$$\delta r_{i,j,X}^2 + \delta r_{i,j,Y}^2 \leq \Delta \beta_{i,j,XY}^2, \quad (28)$$

$$\delta r_{i,j,Z}^2 \leq \Delta \beta_{i,j,Z}^2, \quad (29)$$

$$\delta t_{i,j,X}^2 + \delta t_{i,j,Y}^2 \leq \Delta b_{i,j,XY}^2, \quad (30)$$

$$\delta t_{i,j,Z}^2 \leq \Delta b_{i,j,Z}^2, \quad (31)$$

Where $\delta \mathbf{r}_{i,j} \equiv [\delta r_{i,j,X} \quad \delta r_{i,j,Y} \quad \delta r_{i,j,Z}]^T$ and $\delta \mathbf{t}_{i,j} \equiv [\delta t_{i,j,X} \quad \delta t_{i,j,Y} \quad \delta t_{i,j,Z}]^T$

3.5.3 Computing the Maximum Moving-Platform Pose Errors

Firstly, it is needed to find the maximum reference-point position error as well as the maximum orientation error of the moving platform due to joint clearances. This is done by solving the problems

$$\begin{aligned} -r_{max}^2 &\equiv \text{minimize} && \sum_{k=1,2,3} (\mathbf{e}_{6,k}^T \delta \mathbf{p})^2, && (32) \\ &\text{over} && \delta \mathbf{p}, \delta \mathbf{s}_{i,j}, j = 1, \dots, n_i, i = 1, \dots, m, \\ &\text{subject to} && (\mathbf{e}_{6,1}^T \delta \mathbf{s}_{i,j})^2 + (\mathbf{e}_{6,2}^T \delta \mathbf{s}_{i,j})^2 \leq \delta \beta_{XY,i,j}^2, \\ &&& (\mathbf{e}_{6,3}^T \delta \mathbf{s}_{i,j})^2 \leq \delta \beta_{Z,i,j}^2, \\ &&& \delta \mathbf{p} = \mathbf{M}_i \delta \mathbf{s}_i, \\ &&& j = 1, \dots, n_i, i = 1, \dots, m. \end{aligned}$$

and

$$\begin{aligned} -p_{max}^2 &\equiv \text{minimize} && \sum_{k=4,5,6} (\mathbf{e}_{6,k}^T \delta \mathbf{p})^2, && (33) \\ &\text{over} && \delta \mathbf{p}, \delta \mathbf{s}_{i,j}, j = 1, \dots, n_i, i = 1, \dots, m, \\ &\text{subject to} && (\mathbf{e}_{6,1}^T \delta \mathbf{s}_{i,j})^2 + (\mathbf{e}_{6,2}^T \delta \mathbf{s}_{i,j})^2 \leq \delta \beta_{XY,i,j}^2, \\ &&& (\mathbf{e}_{6,3}^T \delta \mathbf{s}_{i,j})^2 \leq \delta \beta_{Z,i,j}^2, \\ &&& (\mathbf{e}_{6,4}^T \delta \mathbf{s}_{i,j})^2 + (\mathbf{e}_{6,5}^T \delta \mathbf{s}_{i,j})^2 \leq \delta b_{XY,i,j}^2, \\ &&& (\mathbf{e}_{6,6}^T \delta \mathbf{s}_{i,j})^2 \leq \delta b_{Z,i,j}^2, \end{aligned}$$

$$\begin{aligned}\delta \mathbf{p} &= \mathbf{M}_i \delta \mathbf{s}_i, \\ j &= 1, \dots, n_i, i = 1, \dots, m.\end{aligned}$$

As one can see, the problem for the maximal orientation error can be simplified because orientation error does not depend on the translational positions of the joint. Whereas for the maximal position error, orientation also has an effect on the overall error assessment.

Computing the global optima r_{max} and p_{max} requires some additional effort, because the aforementioned problems are nonconvex quadratically constrained quadratic programs (QCQPs). Firstly, equation (32) needs to be simplified via QR factorizations of \mathbf{M}_i^T ,

$$-\mathbf{M}_i^T = \mathbf{V}_i \mathbf{U}_i, \quad (34)$$

$$\begin{aligned}&= [\mathbf{V}_{i,1} \quad \mathbf{V}_{i,2}] \begin{bmatrix} \mathbf{U}_{i,1} \\ \mathbf{0}_{(6n-6) \times 6} \end{bmatrix}, \\ &= \mathbf{V}_{i,1} \mathbf{U}_{i,1},\end{aligned} \quad (35)$$

where $i = 1, \dots, m$, $\mathbf{V}_i \in \mathbb{R}^{6n_i \times 6n_i}$ is orthogonal and $\mathbf{U}_i \in \mathbb{R}^{6n_i \times 6}$ is upper-triangular, $\mathbf{V}_{i,1} \in \mathbb{R}^{6 \times 6}$, $\mathbf{V}_{i,2} \in \mathbb{R}^{6 \times (6n_i-6)}$ and $\mathbf{U}_{i,1} \in \mathbb{R}^{6 \times 6}$ is an upper-triangular matrix. Defining

$$\delta \mathbf{q}_i \equiv \begin{bmatrix} \delta \mathbf{q}_{i,1} \\ \delta \mathbf{q}_{i,2} \end{bmatrix} = \mathbf{V}_i^T \delta \mathbf{s}_i, \quad (36)$$

where $\delta \mathbf{q}_{i,1} \in \mathbb{R}^6$ and $\delta \mathbf{q}_{i,2} \in \mathbb{R}^{6n_i-6}$ in a way that,

$$\delta \mathbf{s}_i = \mathbf{V}_{i,1} \delta \mathbf{q}_{i,1} + \mathbf{V}_{i,2} \delta \mathbf{q}_{i,2}, \quad (37)$$

allows to rewrite the equality constraints (35) as

$$\delta \mathbf{p} = \mathbf{M}_i \delta \mathbf{s}_i = \mathbf{U}_{i,1}^T \mathbf{V}_{i,1}^T \delta \mathbf{s}_i = \mathbf{U}_{i,1}^T \delta \mathbf{q}_{i,1}, \quad (38)$$

When putting (38) into (37):

$$\delta \mathbf{s}_i = \mathbf{V}_{i,1} \mathbf{U}_{i,1}^{-T} \delta \mathbf{p} + \mathbf{V}_{i,2} \delta \mathbf{q}_{i,2}, \quad (39)$$

Grouping all the remaining optimization variables into an array,

$$\delta \mathbf{u} \equiv [\delta \mathbf{p}^T \quad \delta \mathbf{q}_{1,2}^T \quad \delta \mathbf{q}_{2,2}^T \quad \dots \quad \delta \mathbf{q}_{m,2}^T]^T \in \mathbb{R}^{\mathbf{v}} \quad (40)$$

where $\mathbf{v} = 6 + 6 \sum_{k=1}^m (n_k - 1)$ gives us a possibility to express

$$\delta \mathbf{s}_i \equiv \mathbf{Y}_i \delta \mathbf{u}, \quad (41)$$

and where

$$\mathbf{Y}_i = [\mathbf{V}_{i,1} \mathbf{U}_{i,1}^{-T} \quad \mathbf{V}_{i,2} \quad \mathbf{0}_{6n_i \times 6 \sum_{k=i+1}^m (n_k - 1)}] \in \mathbb{R}^{6n_i \times \mathbf{v}} \quad (42)$$

for $i = 1$

$$\mathbf{Y}_i = [\mathbf{V}_{i,1} \mathbf{U}_{i,1}^{-T} \quad \mathbf{0}_{6n_i \times 6 \sum_{k=i}^{i-1} (n_k-1)} \quad \mathbf{V}_{i,2} \quad \mathbf{0}_{6n_i \times 6 \sum_{k=i+1}^m (n_k-1)}] \in \mathbb{R}^{6n_i \times v} \quad (43)$$

for $i = 2, \dots, m-1$ and

$$\mathbf{Y}_i = [\mathbf{V}_{i,1} \mathbf{U}_{i,1}^{-T} \quad \mathbf{0}_{6n_i \times 6 \sum_{k=i}^{i-1} (n_k-1)} \quad \mathbf{V}_{i,2}] \in \mathbb{R}^{6n_i \times v} \quad (44)$$

for $i = m$

where finally the optimization problem can be overwritten so that it contains only inequality constraints:

$$\begin{aligned} -p_{max}^2 &\equiv \text{minimize} & f_0 &\equiv -\delta \mathbf{u}^T \mathbf{F}_0 \delta \mathbf{u}, & (45) \\ &\text{over} & \delta \mathbf{u}, & \\ &\text{subject to} & f_{i,j,k}(\delta \mathbf{u}) &\equiv \delta \mathbf{u}^T \mathbf{F}_{i,j,k} \delta \mathbf{u} - 1 \leq 0, \\ & & k &= 1, \dots, 4, j = 1, \dots, n_i \\ & & i &= 1, \dots, m. \end{aligned}$$

where

$$\mathbf{F}_0 \equiv \sum_{l=4,5,6} \mathbf{e}_{v,l} \mathbf{e}_{v,l}^T, \quad (46)$$

$$\begin{aligned} \mathbf{F}_{i,j,1} &\equiv (1/\delta \beta_{XY,i,j}^2) \mathbf{Y}_i^T (\mathbf{e}_{6n_i,6j-5} \mathbf{e}_{6n_i,6j-5}^T + \\ &\quad \mathbf{e}_{6n_i,6j-4} \mathbf{e}_{6n_i,6j-4}^T) \mathbf{Y}_i, \end{aligned} \quad (47)$$

$$\mathbf{F}_{i,j,2} \equiv (1/\delta \beta_{Z,i,j}^2) \mathbf{Y}_i^T \mathbf{e}_{6n_i,6j-3} \mathbf{e}_{6n_i,6j-3}^T \mathbf{Y}_i, \quad (48)$$

$$\begin{aligned} \mathbf{F}_{i,j,3} &\equiv (1/\delta b_{XY,i,j}^2) \mathbf{Y}_i^T (\mathbf{e}_{6n_i,6j-2} \mathbf{e}_{6n_i,6j-2}^T + \\ &\quad \mathbf{e}_{6n_i,6j-1} \mathbf{e}_{6n_i,6j-1}^T) \mathbf{Y}_i, \end{aligned} \quad (49)$$

$$\mathbf{F}_{i,j,2} \equiv (1/\delta b_{Z,i,j}^2) \mathbf{Y}_i^T \mathbf{e}_{6n_i,6j} \mathbf{e}_{6n_i,6j}^T \mathbf{Y}_i. \quad (50)$$

The authors solve the optimization problem (45) via ModeFrontier software and through two illustrative examples with a 3R serial and a five-bar parallel manipulator it results that the overall displacements for the serial mechanism are multiple times larger than the five-bar.

3.6 Geometric Analysis of the Kinematic Sensitivity of Planar Parallel Mechanisms

Lastly, we address the proposed kinematic sensitivity index by Saadatzi et al [25] using geometric approach in the case of planar parallel mechanisms. The work is based on the work of P. Cardou et al. [22], discussed in section 3.4. The elliptical and rectangular shapes are used to model in the 2- and ∞ -norm respectively and a planar 3-RPR parallel mechanism is used to

provide numerical examples. In [22] the constraint and objective functions are both in calculated using the same norm. Thus, to add to article Saadatzi et al. try to differ the norms between the constraint and objective functions. The state where the constraint is taken using 2-norm but the objective function is in ∞ -norm is observed first-hand. Using the numerical example where the numerical values are taken using a posture with a Jacobian matrix:

$$\mathbf{K} = \begin{bmatrix} 0.5456 & 0.8380 & 0.0535 \\ -0.8080 & 0.5892 & 0.5892 \\ -0.8588 & -0.5123 & 0.9999 \end{bmatrix}, \quad (51)$$

it is noted that maximal orientational error stays the same, since the operator has only one rotational DOF. For the maximal positioning error though:

$$\sigma_{p_{2,2}} = \sqrt{\|\mathbf{E}_p^{-1}\|_2} = 1.7418, \quad (52)$$

$$\sigma_{p_{2,\infty}} = \max(dx, dy) = 1.6811, \quad (53)$$

where $\sigma_{p_{2,2}}$ and $\sigma_{p_{2,\infty}}$ are the maximal positioning errors having $c=f=2$ and $c=2, f=\infty$ respectively with c being the constraint and f the objective function norm. \mathbf{E} is defined in section 3.4.2 and

$$d_i = \frac{1}{\sqrt{E_i}}, \quad (54)$$

is the farthest distance along the x_i axis.

From this we can see, that using $c=f=2$ accounts for a larger positioning error than mixing the norms. The author shows all of the variations geometrically via Figure 7. From the illustration it can be concluded that

$$\sigma_{\infty,2} \geq \sigma_{\infty,\infty} \geq \sigma_{2,\infty}, \quad \sigma_{\infty,2} \geq \sigma_{2,2} \geq \sigma_{2,\infty}. \quad (55)$$

In reality, there is no such relationship between $\sigma_{\infty,\infty}$ and $\sigma_{2,2}$. According to the illustration, if the constraint ellipsoid or polyhedron rotates, the value of $\sigma_{\infty,\infty}$ and $\sigma_{2,\infty}$ would change, whilst $\sigma_{2,2}$ and $\sigma_{\infty,2}$ stay the same. In addition, the change of coordinates, which alters the Jacobian matrix of the mechanism, should not affect kinematic sensitivity. Thus, it is preferred for the objective function norm to be the 2-norm. Out of the two possibilities and taking Merlet's work [3] into consideration $\sigma_{\infty,2}$ stands out as the most meaningful index for kinematic sensitivities.

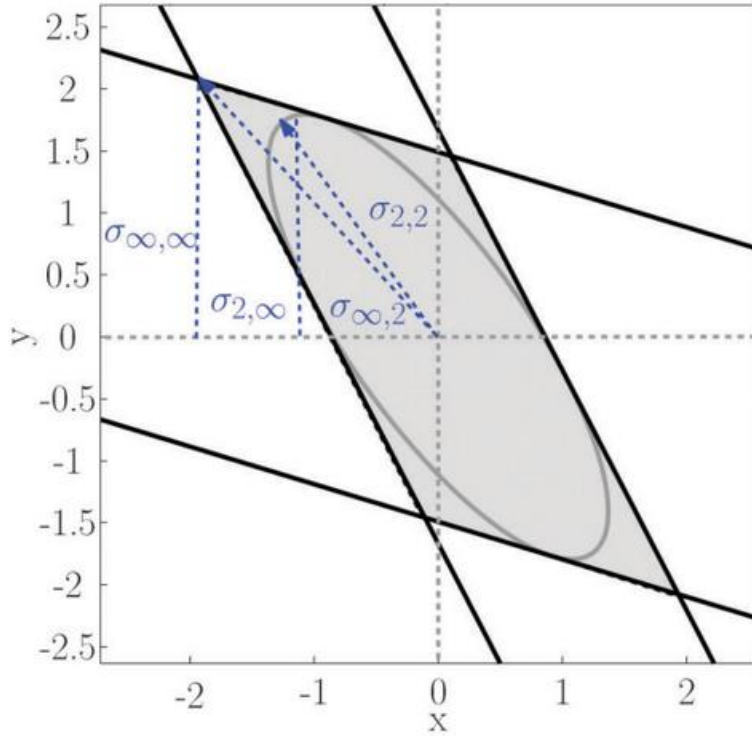


Figure 7 – Geometrical representation of the variations of kinematic sensitivity in the case of a constrained manipulator [25].

In addition, the paper considers redundant manipulators and by doing so, finds that using the 2-norm constraint to calculate kinematic sensitivity becomes invalid. This is because adding redundant limbs also tightens the constraint for the sensitivity ellipse. Thus, the sensitivity of a redundant manipulator can only become smaller in comparison to the former fully actuated non-redundant mechanism, although in reality it might not change. While using the ∞ -norm constraint the constraint might tighten or remain the same. Thus looking at the indices from this perspective the usage of $\sigma_{\infty,2}$ is even more justified.

To add to this, the paper also considers parallel mechanisms with dependent DOF where the Jacobian has the form

$$\begin{bmatrix} \rho \\ \mathbf{0} \end{bmatrix} = \begin{bmatrix} \mathbf{K}_{actuation} \\ \mathbf{K}_{constraint} \end{bmatrix} \mathbf{x}. \quad (56)$$

As we now consider the equation $\mathbf{K}_{constraint} \mathbf{x} = \mathbf{0}$ it becomes possible to overcome the unbounded constraint set which is the main problem in using the ∞ -norm constraint for previous papers. Bounding the formerly unbounded zonotope comes down to computing the intersection of the last row of $\begin{bmatrix} \mathbf{K}_{actuation} \\ \mathbf{K}_{constraint} \end{bmatrix}$ which is a plane in \mathbb{R}^3 .

As shown through an example on the 3-RPR manipulator, where one of the actuators is locked now. According to first-order kinematics, its finite displacements identity may be written as

$$\begin{bmatrix} \boldsymbol{\rho}_1 \\ \boldsymbol{\rho}_1 \\ \mathbf{0} \end{bmatrix} = \begin{bmatrix} n_{1x} & n_{1y} & (b_1 \times n_1) \cdot k \\ n_{2x} & n_{2y} & (b_2 \times n_2) \cdot k \\ n_{3x} & n_{3y} & (b_3 \times n_3) \cdot k \end{bmatrix}, \quad (57)$$

According to

$$\mathbf{L}\Delta\mathbf{x} \preceq \mathbf{1}_6, \quad (58)$$

in which $\mathbf{L} \equiv [\mathbf{K}^T - \mathbf{K}^T]^T$, \preceq denotes the componentwise inequality and

$$\mathbf{1}_6 \equiv [1 \ 1 \ \dots \ 1]^T \in \mathbb{R}^6$$

we can write the constraint in the ∞ -norm as:

$$\begin{bmatrix} 0.5456 & 0.8380 & 0.0535 \\ -0.8080 & 0.5892 & 0.5892 \\ -0.5456 & -0.8380 & -0.0535 \\ 0.8080 & -0.5892 & -0.5892 \end{bmatrix} \begin{bmatrix} x \\ y \\ \phi \end{bmatrix} \preceq \begin{bmatrix} 1 \\ 1 \\ 1 \\ 1 \end{bmatrix}, \quad \text{and} \quad \begin{bmatrix} -0.8588 \\ -0.5123 \\ 0.9999 \end{bmatrix}^T \begin{bmatrix} x \\ y \\ \phi \end{bmatrix} = 0. \quad (59)$$

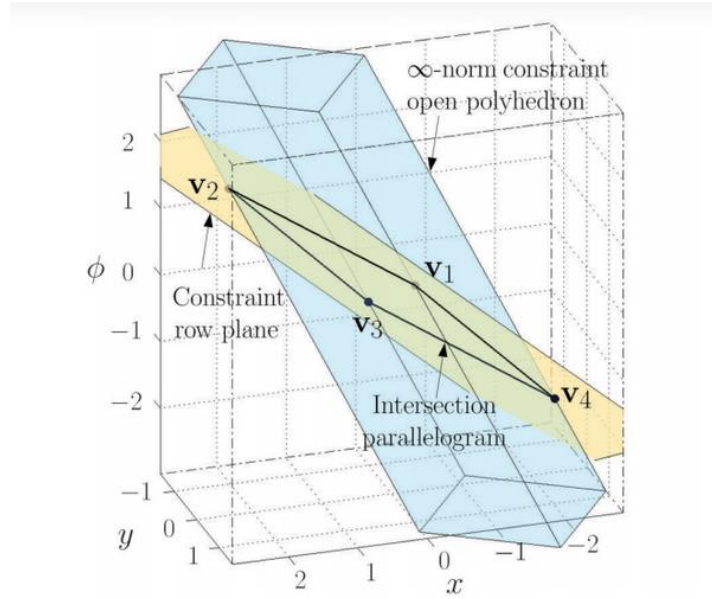


Figure 8 – Geometric representation of the kinematic sensitivity constraints for a 3-RPR parallel manipulator with a locked actuator [25].

The intersecting polyhedron has four vertices. This object is symmetric about origin, thus only two of the four vertices have to be computed. Hence

$$\begin{bmatrix} 0.5456 & 0.8380 & 0.0535 \\ -0.8080 & 0.5892 & 0.5892 \\ -0.8588 & -0.5123 & 0.9999 \end{bmatrix} \begin{bmatrix} x_1 \\ y_1 \\ \phi_1 \end{bmatrix} = \begin{bmatrix} 1 \\ 1 \\ 0 \end{bmatrix} \Rightarrow \mathbf{v}_1 = \begin{bmatrix} 0.0325 \\ 1.1333 \\ 0.6085 \end{bmatrix}, \quad (60)$$

$$\begin{bmatrix} 0.5456 & 0.8380 & 0.0535 \\ 0.8080 & -0.5892 & -0.5892 \\ -0.8588 & -0.5123 & 0.9999 \end{bmatrix} \begin{bmatrix} x_2 \\ y_2 \\ \phi_2 \end{bmatrix} = \begin{bmatrix} 1 \\ 1 \\ 0 \end{bmatrix} \Rightarrow \mathbf{v}_2 = \begin{bmatrix} 2.2279 \\ -0.3674 \\ 1.7253 \end{bmatrix}. \quad (61)$$

while the remaining two vertices are the opposites of \mathbf{v}_1 and \mathbf{v}_2 . The corresponding objective values in the ∞ -norm are

$$\sigma_{p_{\infty,\infty}} = \max\left(\max_{i=1,\dots,4} x_i, \max_{i=1,\dots,4} y_i\right) = \max\left(\max_{i=1,2} |x_i|, \max_{i=1,2} |y_i|\right) = 2.2279, \quad (62)$$

$$\sigma_{p_{\infty,2}} = \max_{i=1,\dots,4} \sqrt{x_i^2 + y_i^2} = \max_{i=1,2} \sqrt{x_i^2 + y_i^2} = 2.2580, \quad (63)$$

$$\sigma_{r_{\infty,\infty}} = \sigma_{r_{\infty,2}} = \max_{i=1,\dots,4} \phi_i = \max_{i=1,2} |\phi_i| = 1.7253. \quad (64)$$

The paper concludes with a push towards finding a global performance index through kinematic sensitivity, but is not able to find a robust method due to the possibility of a mechanism having singular poses within its workspace. Mechanisms are not comparable once singular poses occur since the location of said poses within the workspace varies. One workaround is using methods like dimensional-synthesis, which would exclude singular poses, but, in general, it is impossible to avoid singularity.

4 Recent work

A simulation carried out by B. Lian et al. [26], which discusses parameter sensitivity of a 5-DoF parallel manipulator is taken as an example. The T5 PM, which will be used in the analysis is a friction stir welding robot that, due to its high accuracy, pressure tolerances and complex build, is finding interest in the industry and research community alike. Insight on the practices used and the process of the simulation is presented. In addition, results are presented and an analysis is presented at the end of the section.

4.1 Parameter sensitivity analysis of a 5-DoF parallel manipulator

As stated in [26], the analysis of parameters with respect to performance has been a staple for deciding if PMs satisfy engineering requirements. Due to parallel manipulators regularly having large numbers of parameters, finding out what effects they have on performance is crucial. In general, parameter sensitivity is the method of understanding how the change of variables impacts output. Usually performance is measured by kinematic sensitivity, otherwise known as accuracy sensitivity, and two ways are used: the analytical and probabilistic

approach. Last of which is used in this paper, due to its capability of considering large numbers and different types of parameters efficiently. This approach is usually handled in two ways. Either with the Monte Carlo simulation or using a response surface model. Since the former does not take coupling of the parameters in account, the latter is used.

To ensure correctness of the analysis, performance reliability is introduced to study the probability of PMs achieving expected performance. In this way, mean value and variance are taken into account in the analysis to increase accuracy and practicality.

1.1.1 The Response Surface Method

The idea of a response surface model is to match mathematical models with experimental results. The choice of response surface is crucial in the analysis and it is implemented with the following stages:

- 1) Determine parameters and performance response
- 2) Select experimental design strategy and execute design experiments
- 3) Obtain response model and assess its accuracy.

The first of which is discussed in paragraph 4.1.1. Four options are regarded for the experimental design strategy. Full or fractional factorial design (FFD), central composite design (CCD), box Behnken design (BBD) and Latin hypercube design (LHD). Of these options LHD is used due its features of involving coupling and having a limited amount of design experiments to work with, regardless of the amount of parameters thus making it computationally less heavy to use.

The response model is obtained using the least square method and linear, quadratic and cubic orders are considered as candidates. The appropriate model is chosen in reference to accuracy which is assessed using four metrics:

$$\begin{aligned}
 RS &= 1 - \frac{\sum_{i=1}^m (y_i - \hat{y}_i)^2}{\sum_{i=1}^m (y_i - \bar{y})^2}, \text{RAAE} = \frac{\sum_{i=1}^m |y_i - \hat{y}_i|}{\sum_{i=1}^m |y_i - \bar{y}|}, \\
 \text{RMAE} &= \frac{\max\{|y_1 - \hat{y}_1|, \dots, |y_m - \hat{y}_m|\}}{\frac{\sum_{i=1}^m |y_i - \bar{y}|}{m}}, \\
 \text{RMSE} &= \sqrt{\frac{\sum_{i=1}^m (y_i - \bar{y})^2}{m}}
 \end{aligned} \tag{65}$$

R Square (RS), Relative Average Absolute Error (RAAE), Root Mean Square Error (RMSE) namely are used to evaluate accuracy departments. The sampling points for subsystem I, with the number of experiments for the first, second and third orders of surface models being 42, 462, 502 and the error analysing points being 21, 231, 251, respectively. Corresponding accuracy assessments are shown in Table 2. The respective points for subsystem II are 40, 420 and 458, with error analysing points being 20, 210 and 229 accordingly. The accuracy assessment for subsystem II is shown in Table 3.

4.1.1 Determination of variables and performance

To start with, the parameters and sought performance has to be described and defined. As defined in [26], the T5 PM is divided into subsystems I and II, containing 20 and 19 parameters respectively. Figures Figure 9-Figure 11 illustrate the build and parameters of the manipulator. One can see that the redundant substructure I and over-constrained substructure II are interlinked by R joints. Thus, the compliance of the end reference point is the superposition of the two substructures.

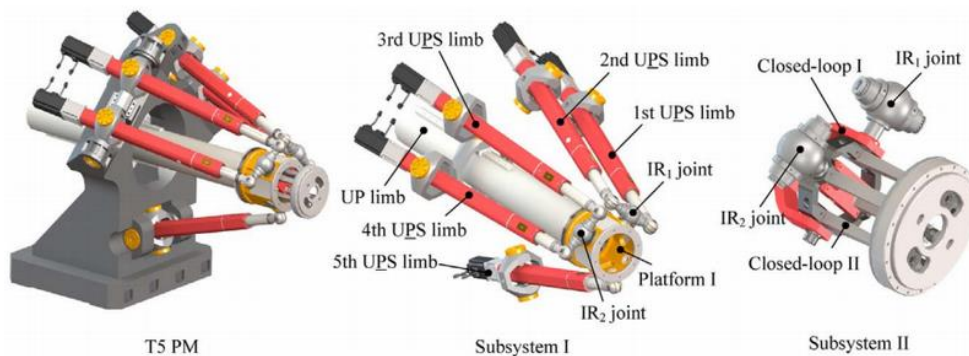


Figure 9 –T5 PM and its Subsystems [26]

4.1.2 Parameter definitions for substructure I

Subsystem I consists of one fixed base, five UPS limbs, one UP limb, two interlinked R joints (IR), and platform I. The 1st and 2nd UPS limbs connect to platform I through IR₁ joint, while the 3rd and 4th UPS limbs link to platform I by IR₂ joint as can be seen from Figure 9. The 5th UPS limb and UP limb attach to platform I directly. Thus, parameters of subsystem I can be divided into four groups: the 1st to 4th UPS limbs, IR joints, the 5th UPS limb, UP limb. According to the structure of the four groups in subsystem I, all possible sectional parameters and related joint stiffness coefficient are shown in Figure 10. For the 1st to 4th UPS limbs, k_u

denotes the stiffness coefficient of U joint along the direction of P joint and d_s represents the screw diameter. D_{op} and d_{op} are the external and internal diameters of the outer pipe, while D_{ip} and d_{ip} are the external and internal diameters of the inner pipe. k_s denotes the stiffness coefficient of S joint along the direction of P joint. For the IR joints with structure of ‘T’ letter, D_{ir1} and d_{ir1} represent the external and internal diameters of the horizontal part of IR joints whereas d_{ir2} stands for the diameter of the vertical part. For the 5th UPS limb, the concerned parameters are with the same meaning as that of the 1st to 4th UPS limbs, distinguished by extra subscript ‘5’. For UP limb, k_U, k_V denote the stiffness coefficients of central U joint. D_{ct} and d_{ct} are the external and internal diameters of central tube. Altogether subsystem I has 20 parameters.

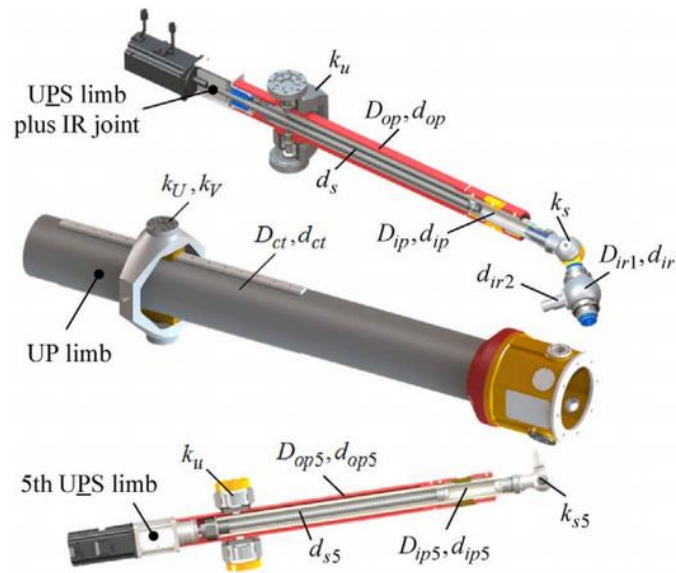


Figure 10 – Structure and parameters of Subsystem I [26]

4.1.3 Parameter definitions for substructure II

As stated in [27], subsystem II is composed of parallelogram-based closed-loop I and closed-loop II. By regarding platform I from subsystem I as the fixed base, IR₁ and IR₂ joints are treated as the actuated joints of subsystem II. Closed-loop I consists of the 1st bracket, the 1st and 2nd rods, and the moving platform whereas closed-loop II is made up of the 2nd bracket, the 3rd and 4th rods, and plate II. The two closed-loops are articulated by one R joint. According to the structure of the closed-loop I and II in subsystem II, all possible sectional parameters and related joint compliance coefficient are shown in Figure 11. The main features of components in closed-loop I and II are extracted as the beam elements drawn by the black lines. a_{ij} ($i = 1\sim 5$ when $j = 1$; $i = 1\sim 3$ when $j = 2$) denotes the shorter edges of cross section, and b_{hj} ($h = 1\sim 3$

when $j = 1$; $h = 1, 2$ when $j = 2$) represents the longer edges of the cross section. $c_{11}, c_{21}, c_{31}, c_{41}, c_{51}$ are the compliance coefficients of the U joints. Overall, subsystem II contains 19 parameters.

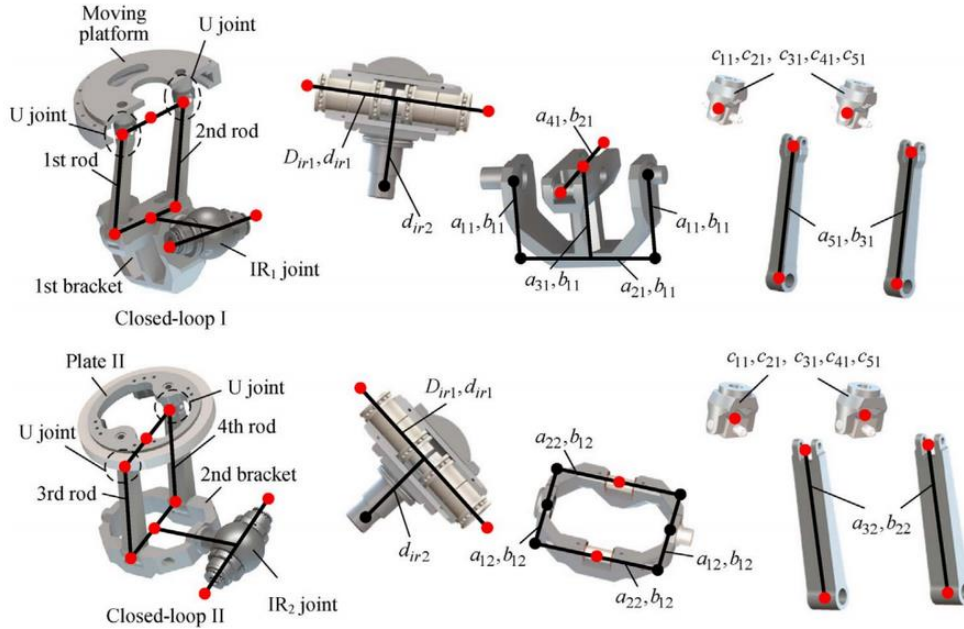


Figure 11 – Structure and parameters of subsystem II [26]

The initial sectional parameters and joint stiffness coefficients are obtained from a virtual prototype and the values of these variables will change between $\pm 10\%$ and $\pm 30\%$, respectively. In addition, performance is determined as mass (M), instantaneous linear stiffness performance ($\eta_{lx}, \eta_{ly}, \eta_{lz}$) and the overall stiffness performance (η) of subsystems I and II. In order to evaluate parameter sensitivity, the targeted performance to parameter mean value and variance is considered. Performance reliability, which describes the probability of PMs achieving desired performance, is used for the task.

$$R = \int_{g(\mathbf{X}) > 0} p(\mathbf{X}) d\mathbf{X} \quad (66)$$

Where, R is the performance reliability, $g(\mathbf{X})$ stands for performance state function and $p(\mathbf{X})$ represents the probabilistic density function of \mathbf{X} .

The state function shows the safe or failure state of the PM system, which can be defined by the performance function obtained by the response surface method.

$$g(\mathbf{X}) = f_U - f(\mathbf{X}) \quad (67)$$

Where f_U denotes the upper performance limits from the engineering requirements. Currently the maximum value within the described workspace is considered the upper limit. The

reliability sensitivity can be achieved by the differentiation of mean value and variance of $g(\mathbf{X})$. If μ_j, σ_j^2 are mean value and variance of x_j ($x_j \in \mathbf{X}, j = 1, 2, \dots, n$), their vector and matrix of \mathbf{X} , respectively can be computed.

$$E(\mathbf{X}) = [\mu_1 \ \mu_2 \ \dots \ \mu_n]^T = \boldsymbol{\mu}, \text{Cov}(\mathbf{X}) = \text{diag}(\sigma_1^2 \ \sigma_2^2 \ \dots \ \sigma_n^2) \quad (68)$$

The state function at point $\mathbf{X} = \boldsymbol{\mu}$ is expressed as

$$g(\mathbf{X}) = g(\boldsymbol{\mu}) + \left. \frac{\partial g(\mathbf{X})}{\partial \mathbf{X}^T} \right|_{\mathbf{X}=\boldsymbol{\mu}} (\mathbf{X} - \boldsymbol{\mu}) + \left. \frac{H(g(\mathbf{X}))}{2!} \right|_{\mathbf{X}=\boldsymbol{\mu}} (\mathbf{X} - \boldsymbol{\mu})^T (\mathbf{X} - \boldsymbol{\mu}) \quad (69)$$

where $\left. \frac{\partial g(\mathbf{X})}{\partial \mathbf{X}^T} \right|_{\mathbf{X}=\boldsymbol{\mu}} = \left[\left. \frac{\partial g(\mathbf{X})}{\partial x_1} \right|_{\mathbf{X}=\boldsymbol{\mu}} \ \left. \frac{\partial g(\mathbf{X})}{\partial x_2} \right|_{\mathbf{X}=\boldsymbol{\mu}} \ \dots \ \left. \frac{\partial g(\mathbf{X})}{\partial x_n} \right|_{\mathbf{X}=\boldsymbol{\mu}} \right]$, and $H(g(\mathbf{X}))$ is the Hessian matrix. Using

these, the mean value and variance of the state function $g(\mathbf{X})$ is calculated as

$$\mu_g = E g(\mathbf{X}) = g(\boldsymbol{\mu}) + \frac{1}{2} \sum_{j=1}^n \sigma_j^2 \left. \frac{\partial^2 g(\mathbf{X})}{\partial x_j^2} \right|_{\mathbf{X}=\boldsymbol{\mu}} \quad (70)$$

$$\begin{aligned} \sigma_g^2 = E(g(\mathbf{X}))^2 - \mu_g^2 &= \sum_{j=1}^n \sigma_j^2 \left\{ \left[\left. \frac{\partial g(\boldsymbol{\mu})}{\partial x_j} \right]^2 - g(\boldsymbol{\mu}) \frac{\partial^2 g(\boldsymbol{\mu})}{\partial x_j^2} \right\} \\ &\quad - \frac{1}{4} \left[\sum_{j=1}^n \sigma_j^2 \left. \frac{\partial^2 g(\boldsymbol{\mu})}{\partial x_j^2} \right]^2 \right\} \end{aligned} \quad (71)$$

where $\left. \frac{\partial g(\boldsymbol{\mu})}{\partial x_j} \right|_{\mathbf{X}=\boldsymbol{\mu}} = \left. \frac{\partial g(\mathbf{X})}{\partial x_j} \right|_{\mathbf{X}=\boldsymbol{\mu}}$, $\left. \frac{\partial^2 g(\boldsymbol{\mu})}{\partial x_j^2} \right|_{\mathbf{X}=\boldsymbol{\mu}} = \left. \frac{\partial^2 g(\mathbf{X})}{\partial x_j^2} \right|_{\mathbf{X}=\boldsymbol{\mu}}$. For further simplification, $\beta = \mu_g / \sigma_g$ denotes

the reliability index and a random variable $Y = [g(\mathbf{X}) - \mu_g] / \sigma_g$ is introduced to the reliability equation. Y is standard to normal distribution and $Y \sim N(0, 1)$. Thus (66) can be rewritten as

$$R = P\{g(\mathbf{X}) > 0\} = 1 - P\{Y \leq -\beta\} = \Phi(\beta) = \frac{1}{\sqrt{2\pi}} \int_{-\infty}^{\beta} e^{-\frac{t^2}{2}} dt \quad (72)$$

From here two values for reliability sensitivity are obtained, one with respect to parameter mean value

$$\begin{aligned}
\frac{\partial R}{\partial \boldsymbol{\mu}} &= \frac{\partial R}{\partial \beta} \frac{\partial \beta}{\partial \mu_g} \frac{\partial \mu_g}{\partial \boldsymbol{\mu}} = \\
&= \frac{1}{\sigma_g} \frac{dR}{d\beta} \left(\frac{\partial g(\boldsymbol{\mu})}{\partial \mu_1} + \frac{1}{2} \sum_{j=1}^n \sigma_j^2 \frac{\partial}{\partial \mu_1} \left[\frac{\partial^2 g(\mathbf{X})}{\partial x_j^2} \Big|_{\mathbf{x}=\boldsymbol{\mu}} \right] \right), \\
&\frac{\partial g(\boldsymbol{\mu})}{\partial \mu_2} + \frac{1}{2} \sum_{j=1}^n \sigma_j^2 \frac{\partial}{\partial \mu_2} \left[\frac{\partial^2 g(\mathbf{X})}{\partial x_j^2} \Big|_{\mathbf{x}=\boldsymbol{\mu}} \right], \dots, \\
&\left. \frac{\partial g(\boldsymbol{\mu})}{\partial \mu_n} + \frac{1}{2} \sum_{j=1}^n \sigma_j^2 \frac{\partial}{\partial \mu_n} \left[\frac{\partial^2 g(\mathbf{X})}{\partial x_j^2} \Big|_{\mathbf{x}=\boldsymbol{\mu}} \right] \right\}^T \\
&\approx \frac{e^{-\frac{\beta^2}{2}}}{\sigma_g \sqrt{2\pi}} \left[\frac{\partial g(\boldsymbol{\mu})}{\partial \mu_1}, \frac{\partial g(\boldsymbol{\mu})}{\partial \mu_2}, \dots, \frac{\partial g(\boldsymbol{\mu})}{\partial \mu_n} \right]^T
\end{aligned} \tag{73}$$

and the other with respect to parameter variance matrix

$$\begin{aligned}
\frac{\partial R}{\partial Cov(\mathbf{X})} &= \frac{\partial R}{\partial \beta} \frac{\partial \beta}{\partial \sigma_g^2} \frac{\partial \sigma_g^2}{\partial Cov(\mathbf{X})} = \\
&= -\frac{\mu_g}{2\sigma_g^3} \frac{dR}{d\beta} \text{diag} \left[\left[\frac{\partial g(\boldsymbol{\mu})}{\partial x_1} \right]^2 - g(\boldsymbol{\mu}) \frac{\partial^2 g(\boldsymbol{\mu})}{\partial x_1^2} - \frac{1}{2} \frac{\partial^2 g(\boldsymbol{\mu})}{\partial x_1^2} \sum_{j=1}^n \sigma_j^2 \frac{\partial^2 g(\boldsymbol{\mu})}{\partial x_j^2}, \right. \\
&\left[\frac{\partial g(\boldsymbol{\mu})}{\partial x_2} \right]^2 - g(\boldsymbol{\mu}) \frac{\partial^2 g(\boldsymbol{\mu})}{\partial x_2^2} - \frac{1}{2} \frac{\partial^2 g(\boldsymbol{\mu})}{\partial x_2^2} \sum_{j=1}^n \sigma_j^2 \frac{\partial^2 g(\boldsymbol{\mu})}{\partial x_j^2}, \dots, \\
&\left. \left[\frac{\partial g(\boldsymbol{\mu})}{\partial x_n} \right]^2 - g(\boldsymbol{\mu}) \frac{\partial^2 g(\boldsymbol{\mu})}{\partial x_n^2} - \frac{1}{2} \frac{\partial^2 g(\boldsymbol{\mu})}{\partial x_n^2} \sum_{j=1}^n \sigma_j^2 \frac{\partial^2 g(\boldsymbol{\mu})}{\partial x_j^2} \right] \\
&\approx -\frac{\mu_g}{2\sigma_g^3} \frac{e^{-\frac{\beta^2}{2}}}{\sqrt{2\pi}} \text{diag} \left[\frac{\partial \sigma_g^2}{\partial \sigma_j^2} \right]
\end{aligned} \tag{74}$$

Reliability sensitivity to parameter mean value shows how the parameter value affects performance reliability while variance shows the effect of the change of parameter value. From these as values, a global index, defined for parameter sensitivity assessment is defined as

$$\epsilon_j = \sqrt{\left(\frac{\kappa_j}{\|\kappa_{\max}\|} \right)^2 + \left(\frac{\delta_j}{\|\delta_{\max}\|} \right)^2}, j = 1, 2, \dots, n \tag{75}$$

where $\kappa_j = \partial R / \partial \mu$, $\delta_j = \partial R / \partial Cov(\mathbf{X})$ and $j = 1, 2, \dots, n$. κ_{\max} and δ_{\max} denote maximum absolute values of parameter sensitivity in terms of mean value and variance.

The author [26] proposes three criteria for evaluating influence of parameter by the reliability sensitivity to parameter mean value as

- 1) **Reliability sensitivity Absolute value (RSAV)**. The absolute values of κ_j indicate the effect degree of mean value of x_i to the performance reliability. Higher absolute value indicates higher sensitivity.
- 2) **Reliability Sensitivity Positive Correlation (RSPC)**. The plus sign of κ_j indicates that the state function increases with the increase of RSAV. Thus, if an upper limit is required, the performance decreases. However, with a lower limit, it shows the same tendency as RSAV
- 3) **Reliability Sensitivity Negative Correlation (RSNC)**. The opposite of RSPC. Higher value indicates better performance if only an upper limit is required.

It can be concluded, that RSAV is suitable in distinguishing main parameters from less meaningful while RSPC and RSNC, although not used in this paper, might carry valuable information for future optimization.

4.1.4 Inverse Position Analysis

In order determine performance response, the compliance matrix of the PM has to be found by solving the Inverse Position Problem. A reference paper by Lian et al. [28] is used to describe this with all of the numerical data taken from Table 4Table **12**, which are gotten from a virtual prototype designed by the authors. The position of the OP is set as

Table 1 – Configuration of the measuring point in frame O -xyz [28]

	x(mm)	y(mm)	z(mm)	$\varphi_x(^{\circ})$	$\varphi_y(^{\circ})$
D	0	0	1200	0	0

To begin with, the description of the schematic diagram, illustrated in Figure 12, of the manipulator is defined,.

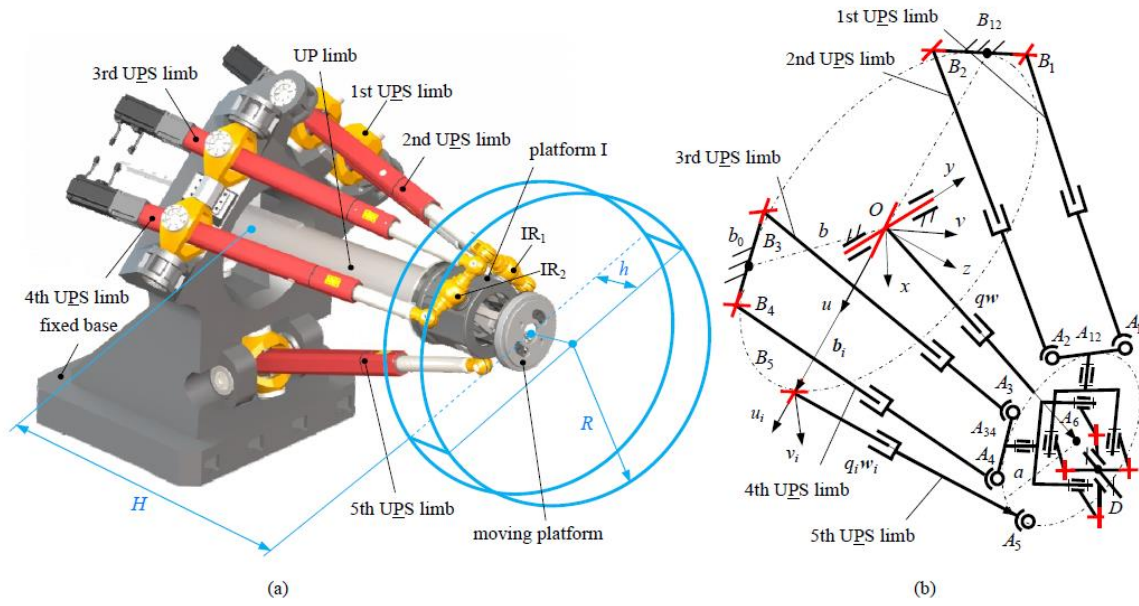


Figure 12 – (a) 3-D model and (b) schematic diagram of T5 PM [28]

As described in [28] and seen in the figure above, the five UPS limbs connect the fixed base by U joints and the 1st and 2nd, 3rd and 4th UPS limbs join platform I together by IR₁ and IR₂, respectively, while the 5th UPS limb links platform I by S joint. The UP limb joins the fixed base by U joint with its centre denoted by point O and connects rigidly to platform I at point A_6 . The prescribed position workspace of T5 PKM is considered as a cylinder whose radius is R and height is h , and the distance between point O and the upper surface of the prescribed workspace is represented by H . Point B_i and A_i denote centres of U joint and S joint of the i^{th} UPS limb ($i = 1 \sim 5$), respectively. The radiuses of the fixed base and the platform I are denoted by b and a , respectively. The point B_{12} , B_{34} are the midpoints of line B_1B_2 and B_3B_4 which are perpendicular to each other, and the distance between B_{12} (or B_{34}) to B_j ($j = 1 \sim 4$) is represented by b_0 . Similarly, point A_{12} , A_{34} are the midpoints of line A_1A_2 and A_3A_4 which are also mutually perpendicular, and the distance between A_{12} (or A_{34}) to A_j ($j = 1 \sim 4$) is denoted by h_0 .

In addition, several reference frame are established. A reference frame $O - xyz$ is fixed to the centre point O with the z -axis normal to the base and the y -axis coincident with the proximal axis of the central U joint. Figure 13 illustrates the additional reference frames of platform I and substructure II.

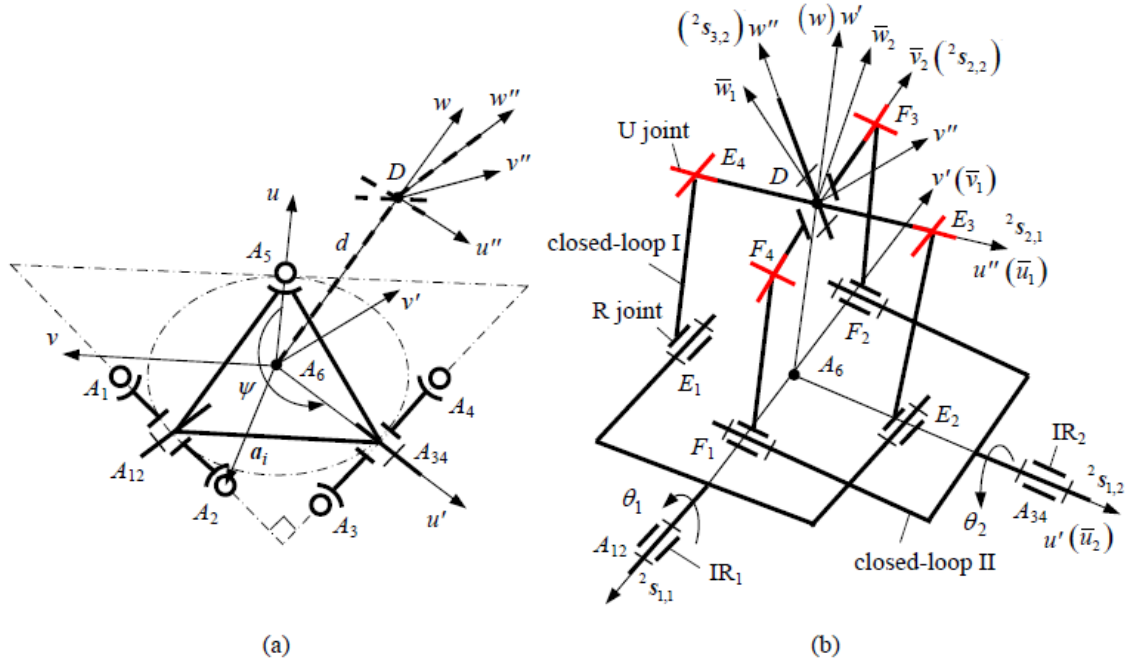


Figure 13 – (a) Description of platform I and (b) schematic diagram of substructure II [28]

As shown, a moving reference frame $A_6 - uvw$ is assigned to the centre point A_6 of platform I. Its u -axis is parallel to the distal axis of central U joint and the w -axis coincides with the axis of P joint of the UP limb. Reference frames $B_i - \bar{u}_i \bar{v}_i \bar{w}_i$ ($i = 1 \sim 5$) shown in Figure 12(b) are defined at point B_i to describe the configuration of UPS limbs, its u_i -axis is collinear with the distal axis of the i^{th} U joint while w_i coincides with the axis of P joint of the i^{th} UPS limb. By rotating frame $A_6 - uvw$ about the w -axis with ψ ($\psi = -5\pi / 4$), the reference frame $A_6 - u'v'w'$ is established at point A_6 . As shown in Figure 13, a reference frame $D - \bar{u}_1 \bar{v}_1 \bar{w}_1$ is set at point D , whose \bar{u}_1 -axis is parallel to line E_3E_4 and the \bar{v}_1 -axis is consistent with the v' -axis. Similarly, a reference frame $D - \bar{u}_2 \bar{v}_2 \bar{w}_2$ is located at point D , whose \bar{u}_2 -axis is collinear with the u' -axis and the \bar{v}_2 -axis is parallel to line F_3F_4 . In addition, a moving reference frame $D - u''v''w''$ is defined with its u'' -axis parallel to line E_3E_4 and the w'' -axis normal to the plane of the moving platform.

Based on the definitions above, orientation matrix \mathbf{R} of frame $A_6 - uvw$ with respect to $O - xyz$ can be described by rotating about y -axis with α angle and u -axis with β angle. The position vector $\mathbf{r} = (x \ y \ z)^T$, of point D in frame $O - xyz$ can be expressed by

$$\mathbf{r} = (q + d)\mathbf{w} \quad (76)$$

where

$$q\mathbf{w} = b_i + q_i\mathbf{w}_i - a_i, i = 1, 2, \dots, 5 \quad (77)$$

herein q and w are the length and unit vector of UP limb, respectively. b_i and a_i represent vectors of point B_i and A_i in frame $O - xyz$. q_i and w_i are the length and unit vector of the i^{th} UPS limb, d is the distance from point A_6 to point D . Since vector a_i is related to the rotations of IR_1 and IR_2 , it can be expressed in frame $O - xyz$ as

$$\mathbf{a}_i = \begin{cases} \mathbf{R}(\mathbf{a}_{10} + \mathbf{R}_\varphi \mathbf{R}_{\theta_1} \mathbf{h}_i), i = 1,2 \\ \mathbf{R}(\mathbf{a}_{20} + \mathbf{R}_\varphi \mathbf{R}_{\theta_2} \mathbf{h}_i), i = 3,4 \\ \mathbf{R}\mathbf{a}_{30}, i = 5 \end{cases} \quad (78)$$

where \mathbf{a}_{10} , \mathbf{a}_{20} , \mathbf{a}_{30} are the vectors of point A_6 to point A_{12} , point A_{34} and point A_5 in frame $A_6 - uvw$, respectively. \mathbf{R}_φ is the orientation matrix of frame $A_6 - u'v'w'$ with respect to frame $A_6 - uvw$. \mathbf{R}_{θ_1} and \mathbf{R}_{θ_2} are the orientation matrixes of IR_1 and IR_2 rotating about v' -axis and u' -axis with θ_1 and θ_2 , respectively. It is worth to mention that \mathbf{R}_{θ_1} and \mathbf{R}_{θ_2} are the orientation matrixes of frame $D - \bar{u}_1\bar{v}_1\bar{w}_1$ and frame $D - \bar{u}_2\bar{v}_2\bar{w}_2$ with respect to frame $A_6 - u'v'w'$, respectively. \mathbf{h}_i (when $i = 1,2,\dots,4$) is the vector from point A_{12} or point A_{34} to A_i in frame $A_6 - uvw$. The orientation matrix of frame $D - u''v''w''$ with respect to frame $A_6 - u'v'w'$ is calculated as

$$\mathbf{R}_\theta = [u'' \quad v'' \quad w''] \quad (79)$$

where $\mathbf{u}'' = \text{Rot}(v', \theta_1)u'$, $\mathbf{w}'' = [\text{Rot}(v', \theta_1)u'] \times [\text{Rot}(u', \theta_2)v']$ and $\mathbf{v}'' = \mathbf{w}'' \times \mathbf{u}''$.

Taken the measuring point D into account matrices \mathbf{R}_{θ_1} and \mathbf{R}_{θ_2} are formulated by

$$\mathbf{w}'' = \mathbf{R}_\varphi^T \mathbf{R}^T \mathbf{w}_6 = (w_x'' \quad w_y'' \quad w_z'')^T \quad (80)$$

where $\theta_1 = \tan^{-1}\left(\frac{w_x''}{w_z''}\right)$ and $\theta_2 = \tan^{-1}\left(-\frac{w_y''}{w_z''}\right)$.

The inverse position problem of T5 PM is solved by calculation of q_i is solved by means of (76) after determining \mathbf{a}_i according to the values of θ_1 and θ_2 .

4.1.5 Stiffness modelling considering gravitational effects

As mentioned, the T5 PM is divided into two structures in which the IR_1 and IR_2 are included by both substructures alike. It is worth mentioning that said joints are considered passive for the first substructure and active for the second. Therefore, the deformation of T5 can be calculated by the sum of deformations of the two substructures in the light of superposition principle. However, the compliance calculation for IR_1 and IR_2 is a challenging task. In addition, gravitational effects are considered as payload.

On the basis of screw theory, the stiffness modelling flow of T5 PM can be concluded as:

- 1) Formulating the wrench and twist mapping models of each substructures considering gravitational effects, after which compliance models in their respective joint space is obtained
- 2) Utilizing virtual work principle and considering deformation compatibility conditions and obtaining compliance models by means of Jacobian matrix.
- 3) Creating the stiffness model of T5 PM, based on deformation superposition principle.

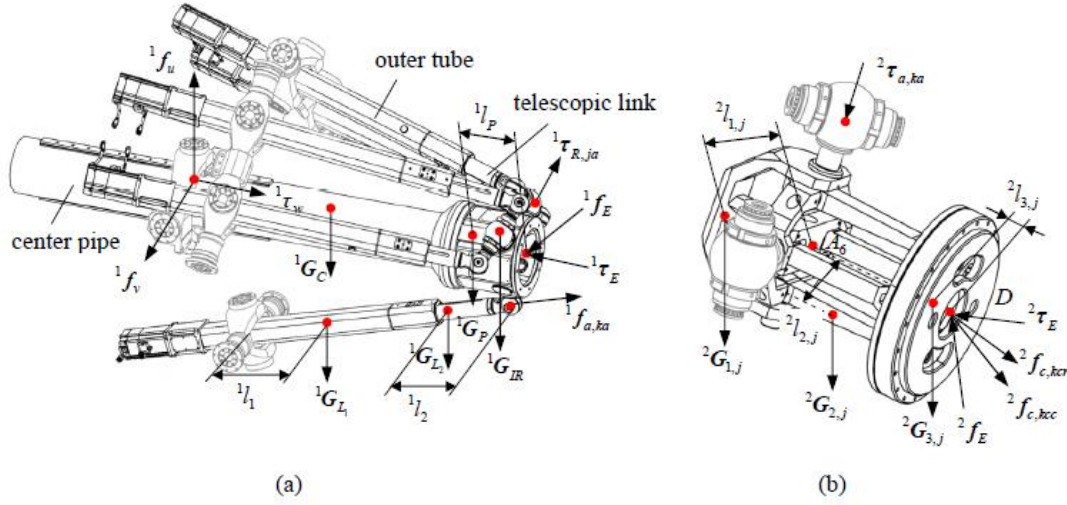


Figure 14 – Free-body diagrams of substructure I (a) and substructure II (b) [28]

4.1.5.1 Wrench mapping model

The wrenches on T5 PM are considered as the external payload and internal payload of actuations/constraints and gravity. Illustrated in the picture above, the equation of static equilibrium of substructure I at point A_6 can be written as

$${}^1\mathcal{W}_{w,E} + {}^1\mathcal{W}_{w,G} = \sum_{ka=1}^5 {}^1f_{a,ka} {}^1\hat{\mathcal{W}}_{wa,ka} - \sum_{ja=1}^2 {}^1\tau_{IRja} {}^1\hat{\mathcal{W}}_{wa,IRja} + \sum_{kc=1}^3 {}^1f_{c,kc} {}^1\hat{\mathcal{W}}_{wc,ka} \quad (81)$$

where ${}^1\mathcal{W}_{w,E}$ represents the external wrench applying on point A_6 , ${}^1\mathcal{W}_{w,G}$ is the equivalent wrench of components applying on point A_6 , ${}^1f_{a,ka}$ and ${}^1\hat{\mathcal{W}}_{wa,ka}$ are the intensity and unit wrench of permission of the ka^{th} limb, ${}^1\tau_{IRja}$ and ${}^1\hat{\mathcal{W}}_{wa,IRja}$ are intensities and unit wrenches of either IR joint. ${}^1f_{c,kc}$ and ${}^1\hat{\mathcal{W}}_{wc,ka}$ represent unit wrenches of constraints and their intensities of the passive UP limb, and

$${}^1\$_{w,E} = \begin{pmatrix} {}^1\mathbf{f}_E \\ {}^1\boldsymbol{\tau}_E \end{pmatrix}, {}^1\$_{w,G} = {}^1\$_{w,G,L_1} + {}^1\$_{w,G,L_2} + \sum_{ja=1}^2 {}^1\hat{\$}_{w,G,IRja} + {}^1\$_{w,G,C} + {}^1\$_{w,G,P}, \quad (82)$$

$${}^1\$_{w,G,L_1} = {}^1m_{L_1}g \sum_{i=1}^5 \left((({}^1l_1 - q_i)\mathbf{w}_i + \mathbf{a}_i) \times \mathbf{e}_1 \right), \quad (83)$$

$${}^1\$_{w,G,L_2} = {}^1m_{L_2}g \sum_{i=1}^5 \left((-{}^1l_2\mathbf{w}_i + \mathbf{a}_i) \times \mathbf{e}_1 \right), \quad (84)$$

$${}^1\hat{\$}_{w,G,IRja} = {}^1m_{IRja}g \left(\mathbf{a}_{i0} \times \mathbf{e}_1 \right), \quad (85)$$

$${}^1\$_{w,G,C} = \rho A_C q g \begin{pmatrix} \mathbf{e}_1 \\ -\frac{1}{2}q\mathbf{w} \times \mathbf{e}_1 \end{pmatrix}, {}^1\$_{w,G,P} = {}^1m_P \begin{pmatrix} \mathbf{e}_1 \\ -{}^1l_P\mathbf{w} \times \mathbf{e}_1 \end{pmatrix}, \quad (86)$$

$${}^1\hat{\$}_{wa,ka} = \begin{pmatrix} \mathbf{w}_i \\ \mathbf{a}_i \times \mathbf{w}_i \end{pmatrix}, {}^1\hat{\$}_{wa,R,ja} = \begin{pmatrix} \mathbf{0} \\ {}^1\boldsymbol{\tau}_{R,ja} \end{pmatrix}, \quad (87)$$

$${}^1\hat{\$}_{wc,1} = \begin{pmatrix} \mathbf{u} \\ -q\mathbf{w} \times \mathbf{u} \end{pmatrix}, {}^1\hat{\$}_{wc,2} = \begin{pmatrix} \mathbf{v} \\ -q\mathbf{w} \times \mathbf{v} \end{pmatrix}, {}^1\hat{\$}_{wc,3} = \begin{pmatrix} \mathbf{0} \\ \boldsymbol{\tau}_w \end{pmatrix}, \quad (88)$$

where ${}^1\mathbf{f}_E$ and ${}^1\boldsymbol{\tau}_E$ represent external force and torque applying on point A_6 . ${}^1\$_{w,G,L_1}$, ${}^1\$_{w,G,L_2}$, ${}^1\hat{\$}_{w,G,IRja}$, ${}^1\$_{w,G,C}$ and ${}^1\$_{w,G,P}$ are equivalent gravitational wrenches of outer tube of the i^{th} UPS limb, inner telescopic link of the i^{th} UPS limb, IR_1 or IR_2 , central pipe of UP limb and platform I exerting on point A_6 , respectively. ${}^1m_{L_1}$ is the mass of the outer tube, \mathbf{e}_1 denotes the unit vector of gravitational acceleration, and 1l_1 represents the distance between the mass centre of the outer tube and that of U joint. ${}^1m_{L_2}$ denotes the mass of the inner telescopic link, and 1l_2 represents the distance from the mass centre of the inner telescopic to that of S joint. ${}^1m_{IRja}$ is the mass of IR_1 or IR_2 . Besides, ρ and A_C are density and sectional area of the centre pipe of UP limb, 1m_P and 1l_P are the mass of platform I and the distance between the mass centre of platform I to point A_6 , respectively.

The wrench for subsystem II and its static equilibrium is formulated similarly:

$${}^2\$_{w,E} + {}^2\$_{w,G} = \sum_{ka=1}^2 {}^2\tau_{a,ka} {}^2\hat{\$}_{wa,ka} + \sum_{kcc=1}^4 {}^2f_{c_{kcc}} {}^2\hat{\$}_{wc,kcc} + \sum_{kcr=1}^3 {}^2f_{c,kcr} {}^2\hat{\$}_{wc,kcr} \quad (89)$$

where ${}^2\$_{w,E}$ and ${}^2\$_{w,G}$ are the external and gravitational wrenches applying to point D and ${}^2\hat{\$}_{wa,ka}$, ${}^2\hat{\$}_{wc,kcc}$, ${}^2\hat{\$}_{wc,kcr}$ represent the unit wrenches of actuation, constraint and over-constraints, respectively. ${}^2\tau_{a,ka}$, ${}^2f_{c_{kcc}}$, ${}^2f_{c,kcr}$ denote the intensities of the aforementioned wrenches accordingly and

$${}^2\$_{w,E} = \begin{pmatrix} {}^2\mathbf{f}_E \\ {}^2\boldsymbol{\tau}_E \end{pmatrix}, {}^2\$_{w,G} = \sum_{j=1}^2 \sum_{i=1}^3 {}^2\hat{\$_{w,G,i,j}}, \quad (90)$$

$${}^2\$_{w,G,1,j} = {}^2m_{1,j}g \begin{pmatrix} \mathbf{e}_1 \\ -({}^2l_{1,j} + d\mathbf{w}') \times \mathbf{e}_1 \end{pmatrix}, \quad (91)$$

$${}^2\$_{w,G,2,j} = {}^2m_{2,j}g \begin{pmatrix} \mathbf{e}_1 \\ \left({}^2l_{2,j} - \frac{1}{2}d\mathbf{w}' \right) \times \mathbf{e}_1 \end{pmatrix}, \quad (92)$$

$${}^2\$_{w,G,3,j} = {}^2m_{3,j}g \begin{pmatrix} \mathbf{e}_1 \\ {}^2l_{3,j} \times \mathbf{e}_1 \end{pmatrix}, \quad (93)$$

$${}^2\$_{wa,1} = \begin{pmatrix} \mathbf{0} \\ {}^2s_{1,1} \end{pmatrix}, {}^2\$_{wa,2} = \begin{pmatrix} \mathbf{0} \\ {}^2s_{2,2} \times {}^2s_{3,2} \end{pmatrix}, \quad (94)$$

$${}^2\hat{\$_{wc,1}} = \begin{pmatrix} {}^2s_{1,1} \\ \mathbf{0} \end{pmatrix}, {}^2\hat{\$_{wc,2}} = \begin{pmatrix} {}^2s_{1,2} \\ \mathbf{0} \end{pmatrix}, {}^2\hat{\$_{wc,3}} = \begin{pmatrix} {}^2s_{1,1} \times {}^2s_{1,2} \\ \mathbf{0} \end{pmatrix}, \quad (95)$$

$${}^2\hat{\$_{wc,4}} = \begin{pmatrix} \mathbf{0} \\ {}^2s_{1,1} \times {}^2s_{1,2} \end{pmatrix}. \quad (96)$$

where ${}^2\mathbf{f}_E$, ${}^2\boldsymbol{\tau}_E$ are external force and torque applying on point D . ${}^2\hat{\$_{w,G,i,j}}$ is the gravitational wrench of i^{th} component exerting on point D . ${}^2m_{i,1}$ represent the mass of link E_1E_2 , E_1E_4 (or E_2E_3), and output link E_3E_4 of closed-loop I, respectively. Similarly ${}^2m_{i,2}$ is the mass of identical links in closed-loop II. ${}^2l_{1,j}$ is the vector from mass centre of link E_1E_2 to point A_6 , and ${}^2l_{2,j}$ the vector from mass centre of E_1E_4 (E_2E_3) or F_1F_4 (F_2F_3) to point D . ${}^2l_{3,j}$ denotes the vector between mass centre of output link E_3E_4 (F_3F_4) and point D . ${}^2s_{i,j}$ are unit axis vectors of 1-DOF joints shown in Figure 13(b).

As can be seen, depending on the subsystem, ${}^2\tau_{a,ka}$ and ${}^1\tau_{IR_ja}$ describe the same joint whilst one is actuated and the other passive, thus are mutually action and reaction force enabling the wrench model of T5 PM be calculated as

$$\$_w = \mathbf{T}^{-T} {}^1\$_w + {}^2\$_w \quad (97)$$

where $\mathbf{T} = \begin{bmatrix} \mathbf{E}_3 & -d[\mathbf{w} \times] \\ \mathbf{0}_{3 \times 3} & \mathbf{E}_3 \end{bmatrix}$, \mathbf{E}_3 denotes 3×3 unit matrix and $[\mathbf{w} \times]$ represents the skew-symmetric matrix relating to vector \mathbf{w} .

4.1.5.2 Twist mapping model

In an earlier article by Song et. al. [29] where the kinematic analysis and optimal design of the T5 PM is carried out for the first time (November 2014). The kinematic performance index is found by means of reciprocal product associated with the wrench screw and twist matrix, allowing to define the stiffness model via Jacobian matrices and will be discussed in section

4.1.6. Optimal design of the manipulator to perform a multi-objective dimensional synthesis using artificial intelligence via a non-dominated sorting genetic algorithm II (NSGA-II) is used. In which the optimization problem

$$\begin{cases} \text{Maximum} & \kappa = f_1(\mathbf{X}) \\ \text{Minimum} & \sigma = f_2(\mathbf{X}) \\ \text{subject to} & g_j \leq 0 \end{cases} \quad (98)$$

also has some added constraints like the stroke of the P joint in the UPS limb being limited to the prescribed workspace

$$q_{i \min} \leq q_i \leq q_{i \max} \quad (99)$$

with q_i equalling the elements of the solution of the inverse kinematic problem (length of the UPS joint). In addition, the structure within the kinematic chains group must be compact.

$$\lambda_k \leq \lambda_b \quad (100)$$

where λ_k, λ_b denote the normalized value of k (in this thesis known as h_0 from Table 4) and b_0 by b . To add to this, the angles between the UPS limb and the R₁ or R₂ joint is restricted to a range.

$$\theta_{\min} \leq \gamma_i \leq \theta_{\max} \quad i = 1,2,3,4 \quad (101)$$

and to avoid interference between the 2nd and 3rd UPS limb their distance must satisfy

$$\Delta \geq D_{link} \quad (102)$$

where D_{link} is the diameter of UPS limb.

As revealed in [29], the compliance model, which is the inverse of the stiffness model is calculated based on screw theory and the virtual work done by the wrench against the twist. Thus, a compliance model from the wrench and twist mapping models can be formulated as

$$\mathbf{C}\$\mathbf{w} \geq \mathbf{\$}_t \quad (103)$$

where \mathbf{C} refers to the compliance matrix of T5 PM. Taking into account that

$$\mathbf{\$}_t = \mathbf{T}^1\mathbf{\$}_t + {}^2\mathbf{\$}_t \quad (104)$$

the compliance matrix can be expressed as

$$\mathbf{C} = \mathbf{T}^1\mathbf{C}\mathbf{T}^T + {}^2\mathbf{C} \quad (105)$$

herein, ${}^1\mathbf{C}$ and ${}^2\mathbf{C}$ are compliance matrices of substructure I and II with respect to point A_6 and D accordingly. It should be noted that in this paper [28], the friction and contact deformation within the joints are ignored, the deformations of the components must satisfy linear

superposition principle and platform I, links E_3E_4 and F_3F_4 are regarded as rigid bodies without deformations.

4.1.6 Computing the stiffness model

To begin with, the stiffness of IR₁ and IR₂ are calculated. As shown in Figure 15, the joints have the shape of the letter “T” and the horizontal parts link to the 1st and 2nd (or 3rd and 4th) UPS limbs at point A_k and A_{k+1} , respectively. The vertical part connects to platform I by rotational components at point $A'_{k,k+1}$ and joins the actuated joints of substructure II at point $A''_{k,k+1}$ rigidly. In addition, the axial forces ${}^1f_{a,k}$ and ${}^1f_{a,k+1}$ caused by UPS limbs apply to the horizontal part of either IR joint, while the force ${}^1f_{p,kr}$ and torque ${}^1\tau_{p,kr}$ caused by platform I exert on point $A'_{k,k+1}$ and torque $-{}^2\tau_{a,kr}$ which is equal to ${}^1\tau_{R,kr}$ caused by substructure II exerts on point $A''_{k,k+1}$ with analogue direction as the rotational axis of either IR joint.

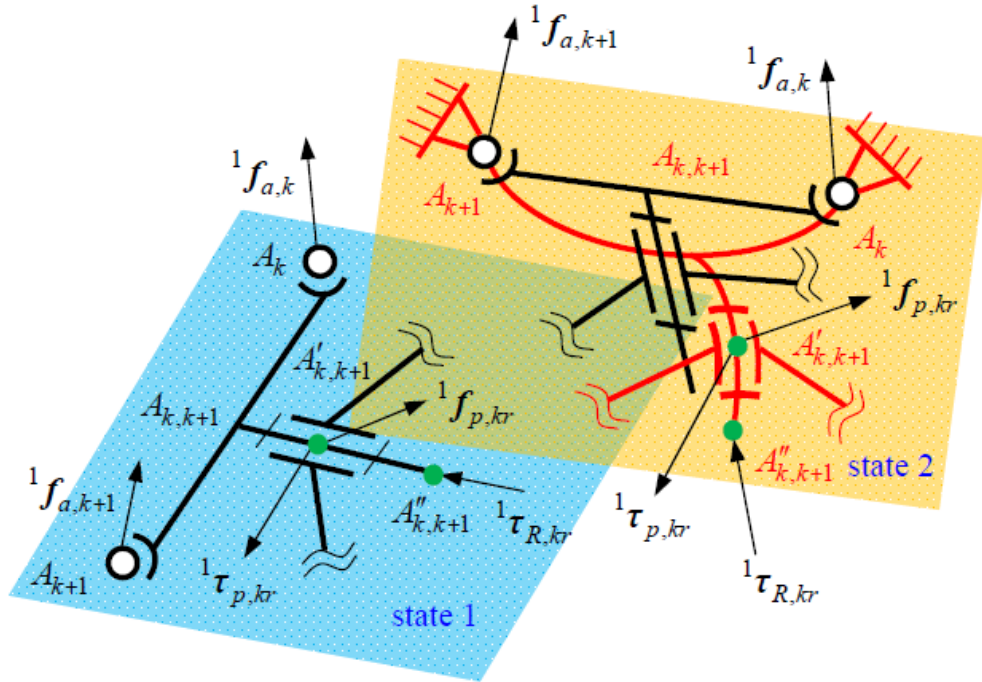


Figure 15 – Force and deformation of IR₁ and IR₂ [28].

Takin the abovementioned into consideration, the compliance of substructure I caused by UPS limbs can be written as follows, when considering the deformation effects of IR joints.

$${}^1C_a = {}^1C_{a,1} + \sum_{i=1}^2 {}^1C_{a,2,i} \quad (106)$$

where ${}^1\mathbf{C}_{a,1}$ is the compliance matrix of substructure I at point A_6 assuming that IR joints are rigid. ${}^1\mathbf{C}_{a,2,i}$ is the compliance matrix caused merely by deformation of the IR joints at the same reference point and can be calculated using finite element analysis (FEA) software. When considering deformation effects on IR joints in substructure II, its compliance matrix

$${}^2\bar{\mathbf{C}}_{ac,j} = {}^2\bar{\mathbf{C}}_{ac1,j} + {}^2\bar{\mathbf{C}}_{ac2,j} \quad (107)$$

where ${}^2\bar{\mathbf{C}}_{ac,j}$ is the actuated compliance matrix of closed loop I and II. ${}^2\bar{\mathbf{C}}_{ac1,j}$ is the compliance matrix of the IR joints at $A'_{k,k+1}$ and can be calculated by ${}^1\mathbf{C}_{a,2,i}$. ${}^2\bar{\mathbf{C}}_{ac2,j}$ refers to the compliance matrix of the component between $A'_{k,k+1}$ and $A''_{k,k+1}$. Again, FEA software based method is applied to obtain reliable results. To determine ${}^2\bar{\mathbf{C}}_{ac2,j}$, platform I is fixed, actuation wrench ${}^2\$_{wa,ka}$ and constrained wrenches ${}^2\$_{wac,kcc}$ and ${}^2\$_{wac,kcr}$ are applied to point $A''_{k,k+1}$. The corresponding translational and orientational displacements, which are the columns of ${}^2\bar{\mathbf{C}}_{ac2,j}$, can be evaluated.

From the fact that the twist at point A_6 can be expressed as follows using the linear superposition principle

$${}^1\$_t = {}^1\$_{ta} + {}^1\$_{tb} + {}^1\$_{tt} = {}^1\mathbf{C}{}^1\$_w \quad (108)$$

where ${}^1\$_{ta}$, ${}^1\$_{tb}$ and ${}^1\$_{tt}$ denote the twist resulted from UPS limbs and IR joints, bending and torsional twists caused by UP limb, respectively. Thus,

$${}^1\mathbf{C} = {}^1\mathbf{C}_a + {}^1\mathbf{C}_b + {}^1\mathbf{C}_t \quad (109)$$

4.1.6.1 Determination of ${}^1\mathbf{C}_a$

Since the forces applying to UPS limbs are only torsion and compression, it allows the compliance of the i^{th} limb at A_i can be formulated as

$$C_{A_i} = \sum_{j=1}^7 C_{a,i,j}, \quad i = 1,2,\dots,5, \quad j = 1,2,\dots,7 \quad (110)$$

where $c_{a,i,1}$ is the axial compliance of S joints. $c_{a,i,2}$, $c_{a,i,3}$, $c_{a,i,4}$, $c_{a,i,5}$ and $c_{a,i,6}$ represent the axial compliance of P joints components including inner telescopic link, screw nut, lead screw, bearings and outer tube, respectively. The numerical values of some these coefficients are shown in Table 6 while components of the limb can be seen from Figure 16. $c_{a,i,7}$ denotes the axial compliance of U joint.

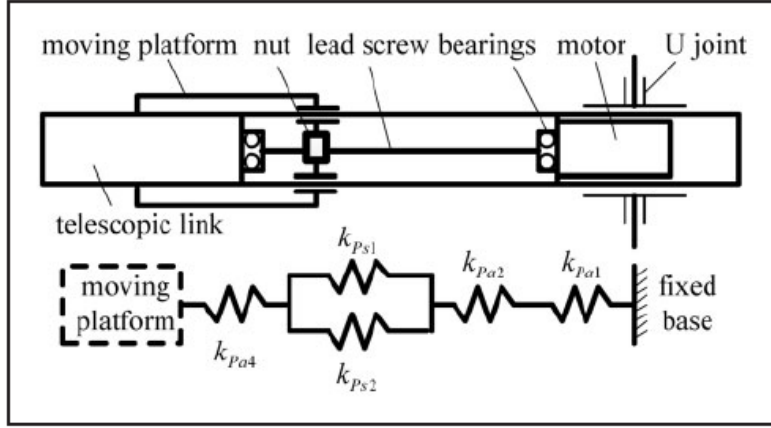


Figure 16 – Components of the P-joint in the \underline{UPS} limb [27].

The S joint of \underline{UPS} limbs is composed of three R joints whose axes are linearly independent and perpendicular mutually. Taking the joint shown in Figure 17 as an example, reference frames $A_{ia} - u_{s,ja}v_{s,ja}w_{s,ja}$ ($ia = 1, 2, \dots, 4$, $ja = 1, 2, 3$) is designated to A_i of the i^{th} \underline{UPS} limb and whose $w_{s,1}$ -axis is collinear with w_{ia} -axis of the ia^{th} \underline{UPS} limb, $u_{s,2}$ -axis is coincident with that of the second R joint and the $v_{s,3}$ -axis coincides with h_{ia} . If $R_{s,ja}$ is the orientation matrix of frame $A_{ia} - u_{s,ja}v_{s,ja}w_{s,ja}$ with respect to frame $A_{ia} - u_{s,ja-1}v_{s,ja-1}w_{s,ja-1}$. Then the orientation matrix of frame $A_{ia} - u_{s,3}v_{s,3}w_{s,3}$ with respect to frame $A_{ia} - u_{s,1}v_{s,1}w_{s,1}$ can be expressed as

$$\mathbf{R}_s = \mathbf{R}_{s,1}\mathbf{R}_{s,2}\mathbf{R}_{s,3} \quad (111)$$

where $\mathbf{R}_{s,1} = \text{Rot}(\mathbf{w}_{s,1}, \theta_{s,1})$, $\mathbf{R}_{s,2} = \text{Rot}(\mathbf{u}_{s,2}, \theta_{s,2})$ and $\mathbf{R}_{s,3} = \text{Rot}(\mathbf{v}_{s,3}, \theta_{s,3})$. $\theta_{s,1}$, $\theta_{s,2}$, and $\theta_{s,3}$ are obtained via Pythagorean theorem from the inverse position analysis in section 4.1.4. In consequence, the 3×3 linear compliance matrix of S joint is formulated as

$$\mathbf{C}_s = \mathbf{C}_{s,1} + \mathbf{C}_{s,2} + \mathbf{C}_{s,3} \quad (112)$$

where $\mathbf{C}_{s,1} = \mathbf{R}_{s,1}\bar{\mathbf{C}}_{s,1}\mathbf{R}_{s,1}^T$, $\mathbf{C}_{s,2} = (\mathbf{R}_{s,1}\mathbf{R}_{s,2})\bar{\mathbf{C}}_{s,2}(\mathbf{R}_{s,1}\mathbf{R}_{s,2})^T$ and $\mathbf{C}_{s,3} = \mathbf{R}_s\bar{\mathbf{C}}_{s,3}\mathbf{R}_s^T$. $\bar{\mathbf{C}}_{s,1}$, $\bar{\mathbf{C}}_{s,2}$ and $\bar{\mathbf{C}}_{s,3}$ denote the linear compliance of three R joints in each reference frame accordingly, see Table 7. It is also noted that the 3rd element of \mathbf{C}_s is the axial linear compliance of S joint, that is $c_{a,i,1}$.

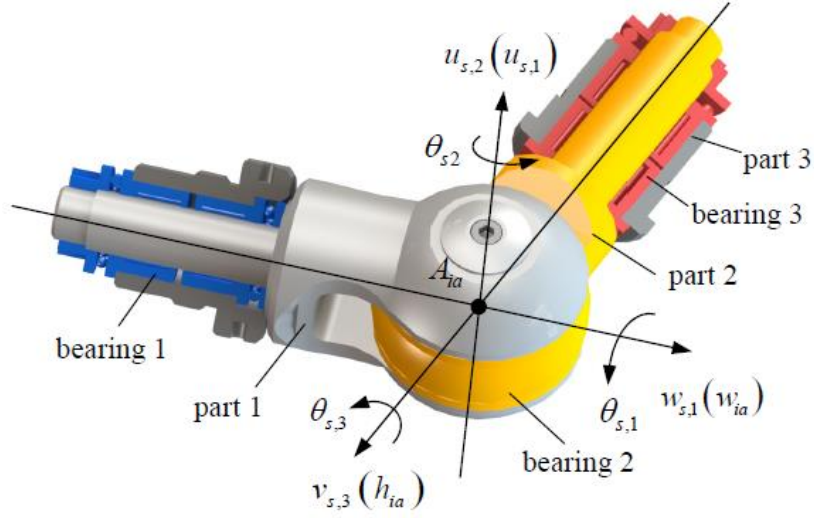


Figure 17 – 3-D model of S joint in the 1st, 2nd, 3rd, and 4th UPS limb [28].

The axial compliance of the lead screw can be determined by the distance between the screw nut and the fixed end as

$$c_{a,i,4} = \frac{q_i - L_{SC}}{EA_{SC}} \quad (113)$$

L_{SC} is the work length, E is the elasticity modulus and A_{SC} is the sectional area of the lead screw. As for the U joint, the 3×3 linear compliance matrix of S joint is formulated as

$$\mathbf{C}_U = \bar{\mathbf{C}}_{in} + \mathbf{R}_U \bar{\mathbf{C}}_{out} + \mathbf{R}_U^T \quad (114)$$

herein, $\bar{\mathbf{C}}_{in}$ and $\bar{\mathbf{C}}_{out}$ are linear compliances of the inner and outer rotational components of the U joint in each reference frame. \mathbf{R}_U is the orientation matrix of the proximal axis with respect to distal axis of U joint. It is noted, that the third element of $diag(\mathbf{C}_U)$ is the axial linear compliance $c_{a,i,7}$.

4.1.6.2 Mapping to point A_6

Now that all of the values for C_{A_i} are obtained, in order to formulate ${}^1\mathbf{C}_a$ they must be mapped into frame A_6 . In the paper referenced earlier [29], the twists of UPS limbs mapping to point A_6 can be described as

$$\mathbf{J}_{xa1} {}^1\mathbf{\$}_{ta} = \mathbf{J}_q \Delta_q \quad (115)$$

where

$${}^1\mathbf{\$}_{ta} = \begin{pmatrix} {}^1\Delta_p \\ {}^1\Delta_\alpha \end{pmatrix}, \quad {}^1\Delta_q = [\Delta q_1 \quad \Delta q_2 \quad \cdots \quad \Delta q_5]^T, \quad (116)$$

$$\mathbf{J}_q = \begin{bmatrix} t_2 & -t_1 & & & \\ & & t_3 & -t_4 & \\ & & & & 1 \end{bmatrix} \quad (117)$$

$$t_1 = {}^1\hat{\$}_{wa,1}^T {}^1\hat{\$}_{ta,R,1}, \quad t_2 = {}^1\hat{\$}_{wa,2}^T {}^1\hat{\$}_{ta,R,1}, \quad t_3 = {}^1\hat{\$}_{wa,3}^T {}^1\hat{\$}_{ta,R,2}, \quad (118)$$

$$t_3 = {}^1\hat{\$}_{wa,3}^T {}^1\hat{\$}_{ta,R,2}, \quad t_4 = {}^1\hat{\$}_{wa,4}^T {}^1\hat{\$}_{ta,R,2}, \quad (119)$$

$$\mathbf{J}_{x\alpha 1} = [\mathbf{J}_{xp1} \quad \mathbf{J}_{x\alpha 1}] = \begin{bmatrix} t_2 \mathbf{w}_1^T - t_1 \mathbf{w}_2^T & (\mathbf{a}_1 \times t_2 \mathbf{w}_1 - \mathbf{a}_2 \times t_1 \mathbf{w}_2)^T \\ t_4 \mathbf{w}_3^T - t_3 \mathbf{w}_4^T & (\mathbf{a}_3 \times t_4 \mathbf{w}_3 - \mathbf{a}_4 \times t_3 \mathbf{w}_4)^T \\ \mathbf{w}_5^T & (\mathbf{a}_5 \times \mathbf{w}_5)^T \end{bmatrix} \quad (120)$$

where ${}^1\Delta_p$ and ${}^1\Delta_\alpha$ denote linear and angular deformations of platform I at point A_6 , Δq_i is the linear deformation of the i^{th} UPS limb, ${}^1\hat{\$}_{ta,R,i}$ are the unit twists of the IR joints. Now the authors [29] used first order perturbation on both side of equation (76) to obtain

$${}^1\Delta_\alpha = \mathbf{T}_{\alpha p} {}^1\Delta_p \quad (121)$$

where $\mathbf{T}_{\alpha p} = \frac{1}{q\mathbf{w}^T \mathbf{w}_e} [\mathbf{w}_e \times] (\mathbf{E}_3 - \mathbf{w}\mathbf{w}^T)$, $\mathbf{w}_e = \mathbf{u} \times \mathbf{e}_2$ and $\mathbf{e}_2 = (0 \quad 1 \quad 0)^T$.

Considering virtual work principle and Hooke's law

$${}^1\hat{\$}_{ta}^T {}^1\hat{\$}_{wa} = \Delta_q^T f_a \quad (122)$$

where ${}^1f_a = {}^1\mathbf{K}_a \Delta_q$ and ${}^1\mathbf{K}_a = \text{diag}(C_{A_1}^{-1}, C_{A_2}^{-1}, \dots, C_{A_5}^{-1})$.

From the aforementioned, we can formulate the deformation contributions of UPS limbs as

$${}^1\mathbf{C}_{a,1} = \mathbf{D}_a (\mathbf{J}_{a1}^T {}^1\mathbf{K}_a \mathbf{J}_{a1})^{-1} \mathbf{D}_a^T \quad (123)$$

Where $\mathbf{D}_a = [\mathbf{E}_3 \quad \mathbf{T}_{\alpha p}^T]^T$ and $\mathbf{J}_{a1} = \mathbf{J}_q^+ (\mathbf{J}_{xp1} + \mathbf{J}_{x\alpha 1} \mathbf{T}_{\alpha p})$. When IR joints are treated as elastic bodies, the compliance matrix of substructure I with respect to point A_6 only caused by IR joint deformations can be calculated as

$${}^1\mathbf{C}_{a,2} = \left(\sum_{j=1}^2 \mathbf{T}_{IR_j}^{-T} \mathbf{K}'_{IR_j} \mathbf{T}_{IR_j}^{-1} \right)^{-1}, \quad j = 1, 2 \quad (124)$$

where $\mathbf{T}_{IR_j} = \begin{bmatrix} \mathbf{R}_{IR_j} & [\mathbf{a}_{IR_j} \times] \mathbf{R}_{IR_j} \\ \mathbf{0} & \mathbf{R}_{IR_j} \end{bmatrix}$, $\mathbf{R}_{IR_j} = \mathbf{R}\mathbf{R}_\psi \mathbf{R}_{\theta_j}$, and $\mathbf{a}_{IR_j} = \mathbf{R}\mathbf{a}_{j0}$

Thus, the compliance matrix ${}^1\mathbf{C}_a$ is achieved by equation (106)

4.1.6.3 Determinations of ${}^1\mathbf{C}_b$ and ${}^1\mathbf{C}_t$

The passive UP limb is exerted by constrained wrenches that can be divided into shearing force or bending moment along or about u -axis and v -axis and the torsional moment about w -axis, which is illustrated in Figure 18. One side of the beam element, that is the UP limb, is named node 1 that is also the centre of U joint. The other side is named node 2 and connects rigidly to platform I. A structure matrix is used to formulate the bending deformation. The element stiffness matrix $\bar{\mathbf{K}}_e$ consists of linear stiffness of U joint $\mathbf{K}_U = \text{diag}(k_{fu1}, k_{fv1})$ and the shearing and bending moment of node 1 is $\mathbf{f}_1 = \mathbf{K}_U \Delta_{p1}$ and $\boldsymbol{\tau}_1 = \mathbf{0}_{2 \times 2}$, where Δ_{p1} refers to the linear deformation of node 1. In consequence, the stiffness matrix of node 2 is formulated as described in [30].

$$\mathbf{K}_{n2} = \mathbf{K}_{22} + \mathbf{K}_{12}^T \left[\begin{bmatrix} \mathbf{K}_U & \mathbf{0} \\ \mathbf{0} & \mathbf{0} \end{bmatrix} - \mathbf{K}_{22} \right]^{-1} \mathbf{K}_{12} \quad (125)$$

where \mathbf{K}_{12} and \mathbf{K}_{22} are the 4×4 sub-matrices of $\bar{\mathbf{K}}_e = \begin{bmatrix} \mathbf{K}_{11} & \mathbf{K}_{12} \\ \mathbf{K}_{12}^T & \mathbf{K}_{22} \end{bmatrix}$

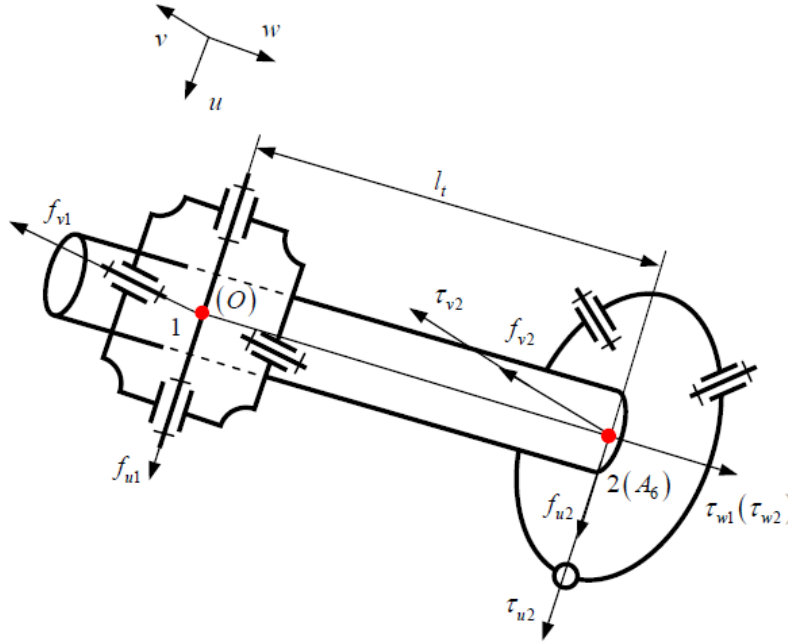


Figure 18 – Free body diagram of the UP limb [28]

Since the position and pose of node 2 must satisfy the deformation compatibility condition, the following equation can be formulated according to equation (115)

$${}^1\$_{tb} = \mathbf{T}_b \begin{pmatrix} \Delta_{p2} \\ \Delta_{\alpha 2} \end{pmatrix} \quad (126)$$

where Δ_{p2} and $\Delta_{\alpha 2}$ denote the linear and angular deformation of node 2, and

$$\mathbf{T}_b = \begin{bmatrix} \mathbf{E}_2 \\ -\mathbf{T}_\alpha^+ \mathbf{T}_p \end{bmatrix}, \mathbf{T}_p = \begin{bmatrix} (t_2 \mathbf{w}_1 - t_1 \mathbf{w}_2)^T \\ (t_4 \mathbf{w}_3 - t_3 \mathbf{w}_4)^T \\ \mathbf{w}_5^T \end{bmatrix} [\mathbf{u} \quad \mathbf{v}], \quad (127)$$

$$\mathbf{T}_\alpha = \begin{bmatrix} (\mathbf{a}_1 \times t_2 \mathbf{w}_1 - \mathbf{a}_2 \times t_1 \mathbf{w}_2)^T \\ (\mathbf{a}_3 \times t_4 \mathbf{w}_3 - \mathbf{a}_4 \times t_3 \mathbf{w}_4)^T \\ \mathbf{a}_5 \times \mathbf{w}_5 \end{bmatrix} [\mathbf{u} \quad \mathbf{v}]$$

Hence we get

$${}^1\mathbf{C}_b = \mathbf{B} \mathbf{T}_b (\mathbf{T}_b^T {}^1\mathbf{K}_{n2} \mathbf{T}_b)^{-1} \mathbf{T}_b^T \mathbf{B}^T \quad (128)$$

where $\mathbf{B} = \begin{bmatrix} [\mathbf{u} \quad \mathbf{v}] & \mathbf{0}_{3 \times 2} \\ \mathbf{0}_{3 \times 2} & [\mathbf{u} \quad \mathbf{v}] \end{bmatrix}$ and ${}^1\mathbf{C}_b$ stands for the bending moment of the UP limb.

The torsional deformation can be obtained by the superposition of the angular deformation of U joint about w -axis and torsional deformation of P joint.

$${}^1\$_{tt} = {}^1\mathbf{C}_t {}^1\$_{wt} \quad (129)$$

where

$${}^1\mathbf{C}_t = \mathbf{T}_t {}^1\mathbf{C}_{wt} \mathbf{T}_t^T, \quad \mathbf{T}_t = \begin{bmatrix} \mathbf{R} & \mathbf{0} \\ \mathbf{0} & \mathbf{R} \end{bmatrix}, \quad {}^1\mathbf{C}_{wt} = \text{diag}(0,0,0,0,0, c_{t1} + c_{t2}) \quad (130)$$

$$c_{t1} = k_{aw,in}^{-1} + (\mathbf{w}_{out}^T \mathbf{K}_{\alpha,out} \mathbf{w}_{out})^{-1}, \quad c_{t2} = \frac{l_t}{GI_t} \quad (131)$$

and, $k_{aw,in}$ is the angular stiffness of proximal axis of U joint about w -axis, $\mathbf{K}_{\alpha,out}$ represents the angular stiffness matrix of the distal axis. \mathbf{w}_{out} is the 3rd column of orientation matrix of distal axis with respect to the proximal axis. l_t stands for torsional length, seen from Figure 18 and GI_t represents the torsional section modulus of the beam element, seen in Table 8.

4.1.6.4 Substructure II

Since substructure II consists of two closed-loops, each loop is viewed separately, after which by means of virtual work principle and Jacobian matrix, the compliance matrix of substructure II is found.

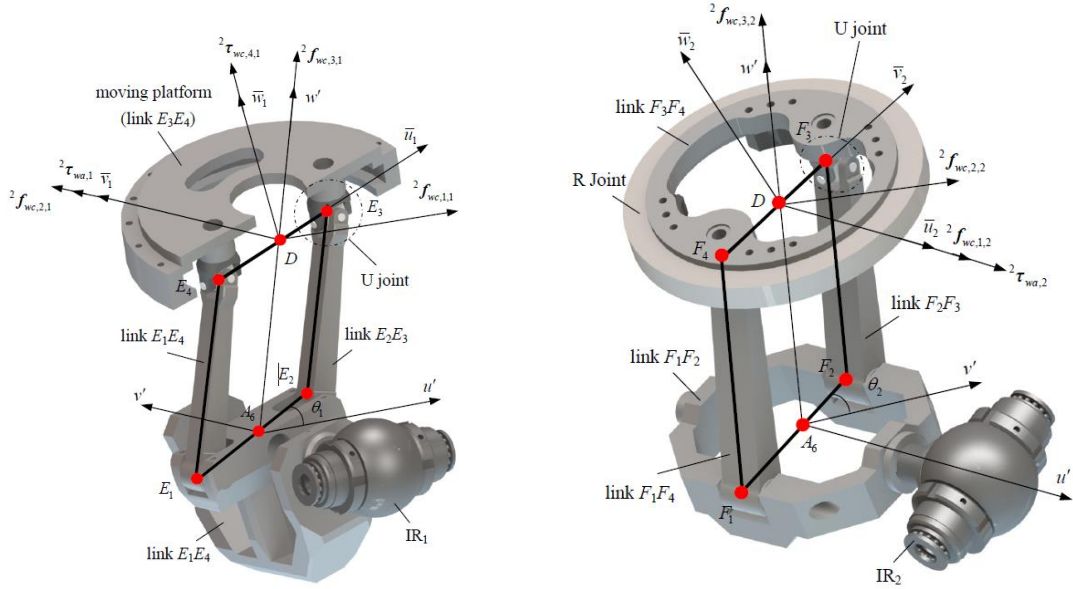


Figure 19 – 3-D model of closed-loop I (left) and II (right) [28]

Beginning with closed-loop I, compliance is formulated through two “roads”, thus the compliance matrix of closed-loop I can be formulated as

$$\begin{cases} {}^2\mathbf{C}_{CL,1,1} = {}^2\bar{\mathbf{C}}_{ac,1} + {}^2\bar{\mathbf{C}}_{1,1} + {}^2\bar{\mathbf{C}}_{2,1} + {}^2\bar{\mathbf{C}}_{3,1} + {}^2\bar{\mathbf{C}}_{5,1} \\ {}^2\mathbf{C}_{CL,2,1} = {}^2\bar{\mathbf{C}}_{ac,1} + {}^2\bar{\mathbf{C}}_{1,1} + {}^2\bar{\mathbf{C}}_{2,1} + {}^2\bar{\mathbf{C}}_{4,1} + {}^2\bar{\mathbf{C}}_{5,1} \end{cases} \quad (132)$$

where ${}^2\bar{\mathbf{C}}_{1,1}$ refers to the compliance matrix of link E_1E_4 from IR_1 to point A_6 . ${}^2\bar{\mathbf{C}}_{2,1}$ is the compliance matrix of E_1E_4 from A_6 to point E_1 or point E_2 , ${}^2\bar{\mathbf{C}}_{3,1}$ and ${}^2\bar{\mathbf{C}}_{4,1}$ denote compliance matrices of link E_1E_4 and E_2E_3 , respectively. ${}^2\bar{\mathbf{C}}_{5,1}$ is the compliance matrix of U joint of closed-loop I.

The virtual work equation of closed-loop I at point D can be obtained as

$${}^2\mathcal{F}_{t,CL1}^T {}^2\mathcal{W}_{w,CL1} = {}^2\mathcal{F}_{t,E_3}^T {}^2\mathcal{W}_{w,E_3} + {}^2\mathcal{F}_{t,E_4}^T {}^2\mathcal{W}_{w,E_4} \quad (133)$$

which can be simplified using the Hooke law,

$${}^2\mathbf{C}_{CL,j,1} {}^2\mathcal{W}_{w,E_i} = {}^2\mathcal{F}_{t,E_i} \quad (134)$$

where, ${}^2\mathcal{F}_{t,D} = \mathbf{T}_{E_i} {}^2\mathcal{F}_{t,E_i}$ is the deformation compatibility conditions of point E_3 and E_4 ,

$$\mathbf{T}_{E_i} = \begin{bmatrix} \mathbf{E}_3 & -[l_{E_i} \times] \\ \mathbf{0} & \mathbf{E}_3 \end{bmatrix}, l_{E_i} \text{ refers to the vector from point } E_i \text{ to point } D \text{ in frame } D - \bar{u}_1 \bar{v}_1 \bar{w}_1$$

where ($j = 1$ for $i = 3$; $j = 2$ for $i = 4$). With this knowledge, the stiffness matrix of closed-loop I in frame $D - \bar{u}_1 \bar{v}_1 \bar{w}_1$ can be formulated as

$${}^2\mathbf{K}_{CL,1} = \sum_{j=1}^2 \mathbf{T}_{E_i}^{-T} {}^2\mathbf{C}_{CL,j,1} \mathbf{T}_{E_i}^{-1} \quad (135)$$

As shown in Figure 19, closed-loop II, similar to closed-loop I is exerted by three forces along \bar{u}_2 , \bar{v}_2 and \bar{w}_2 -axis and one moment about \bar{u}_1 -axis in the local frame $D - \bar{u}_2\bar{v}_2\bar{w}_2$. Closed-loop II also has 2 “roads” from which transformation can transfer to point D . Thus the compliance matrix of closed-loop II considering IR_2 in frame $D - \bar{u}_2\bar{v}_2\bar{w}_2$ can be calculated as

$$\begin{cases} {}^2\mathbf{C}_{CL,1,2} = {}^2\bar{\mathbf{C}}_{ac,2} + {}^2\bar{\mathbf{C}}_{1,2} + {}^2\bar{\mathbf{C}}_{2,2} + {}^2\bar{\mathbf{C}}_{3,2} + {}^2\bar{\mathbf{C}}_{5,2} \\ {}^2\mathbf{C}_{CL,2,2} = {}^2\bar{\mathbf{C}}_{ac,2} + {}^2\bar{\mathbf{C}}_{1,2} + {}^2\bar{\mathbf{C}}_{2,2} + {}^2\bar{\mathbf{C}}_{4,2} + {}^2\bar{\mathbf{C}}_{5,2} \end{cases} \quad (136)$$

where the variables have the same meaning as in closed-loop I, but having F -links instead of E -links. Since the rest of calculations are also the same, just containing links with a different name, the stiffness matrix of closed-loop II in frame $D - \bar{u}_2\bar{v}_2\bar{w}_2$ can be formulated as

$${}^2\mathbf{K}_{CL,2} = \sum_{j=1}^2 \mathbf{T}_{CL,2}^{-T} \mathbf{T}_{F_i}^{-T} {}^2\mathbf{C}_{CL,j,2}^{-1} \mathbf{T}_{E_i}^{-1} \mathbf{T}_{CL,2}^{-1} \quad (137)$$

The only difference in the calculation of the two stiffness matrices is that in closed-loop II, compliance matrix ${}^2\bar{\mathbf{C}}_{F_3F_4}$ which considers link F_3F_4 is not added in the primary equation since it is a moving platform. Thus, it is added later to the stiffness matrix

$${}^2\mathbf{K}_{CL,2} = \left({}^2\bar{\mathbf{K}}_{CL,2}^{-1} + {}^2\bar{\mathbf{C}}_{F_3F_4} \right)^{-1} \quad (138)$$

On the basis of Jacobian matrices of closed-loop I, II and Hooke’s law, the compliance matrix of substructure II at point D without moving platform in frame $D - u'v'w'$ can be described by

$${}^2\bar{\mathbf{C}} = \left(\sum_{i=1}^2 \mathbf{J}_{CL,i}^T {}^2\mathbf{K}_{CL,i} \mathbf{J}_{CL,i} \right)^{-1} \quad (139)$$

where

$$\mathbf{J}_{CL,1} = \begin{bmatrix} {}^2\mathbf{s}_{1,2}^T & 0 \\ {}^2\mathbf{s}_{1,1}^T & 0 \\ ({}^2\mathbf{s}_{1,2} \times {}^2\mathbf{s}_{1,1})^T & {}^2\mathbf{s}_{1,1}^T \\ 0 & ({}^2\mathbf{s}_{1,2} \times {}^2\mathbf{s}_{1,1})^T \\ 0 & 0 \end{bmatrix}, \quad (140)$$

$$\mathbf{J}_{CL,2} = \begin{bmatrix} {}^2\mathbf{s}_{1,2}^T / ({}^2\mathbf{s}_{2,2} \times {}^2\mathbf{s}_{3,2}) & 0 \\ {}^2\mathbf{s}_{1,1}^T / ({}^2\mathbf{s}_{2,2} \times {}^2\mathbf{s}_{3,2}) & 0 \\ ({}^2\mathbf{s}_{1,2} \times {}^2\mathbf{s}_{1,1})^T / ({}^2\mathbf{s}_{2,2} \times {}^2\mathbf{s}_{3,2}) & {}^2\mathbf{s}_{1,2}^T / ({}^2\mathbf{s}_{2,2} \times {}^2\mathbf{s}_{3,2}) \\ 0 & 0 \end{bmatrix} \quad (141)$$

Now the compliance matrix of moving platform ${}^2\bar{\mathbf{C}}_{E_3E_4}$ is considered via linear superposition principle and the compliance matrix of substructure II is derived as

$${}^2\mathbf{C} = {}^2\bar{\mathbf{C}} + \mathbf{T}_{R\theta} {}^2\bar{\mathbf{C}}_{E_3E_4} \mathbf{T}_{R\theta}^T \quad (142)$$

where $\mathbf{T}_{R\theta} = \begin{bmatrix} \mathbf{R}_\theta & \mathbf{0} \\ \mathbf{0} & \mathbf{R}_\theta \end{bmatrix}$.

4.1.7 The results

The following section points out the results of the parameter sensitivity analysis of the T5 PM as presented in [26]. As mentioned earlier, the parameters are grouped into two subsystems and will be considered separately. Absolute values for subsystem I and II are shown (RSAV) in Table 13 and Table 14 and are visualized via Figure 20 and Figure 21, respectively.

In subsystem I, the mass of the objects has a large effect on the stiffness performance of the manipulator, especially parameters involving spherical joints of the UPS limbs. d_s and d_{s5} for example account for 33% of the performance reliability in the overall stiffness performance of the manipulator. It can be seen, that the UP limbs, other than the mass of the manipulator, has little effect on the performance of T5 PM. This could be because it is a passive joint and thus having lesser impact on the performance. Overall, looking at the numerical values and figures, taking overall performance in all areas into account, the main parameters of subsystem I can be determined as: $D_{op}, d_s, D_{ip}, k_s, D_{ct}, d_{ct}, d_{ir2}, d_{s5}, k_{s5}$

For subsystem II, there is a clear difference between mass and stiffness performance. With the top 4 parameters for mass performance being $a_{11}, c_{31}, a_{21}, b_{12}$. Interestingly, c_{31} as a compliance coefficient is among structural parameters in here. This is because reliability of M_2 showed large value towards the variance of c_{31} . Taking both mass and stiffness into account, the main parameters of subsystem II can be determined as $a_{11}, a_{21}, b_{12}, c_{11}, c_{21}, c_{31}$.

5 Analysis and comparison of indices

As seen from the previous sections, researchers have been able to solve the problem of finding kinematic sensitivity indices for parallel manipulators, albeit with some exceptions. It has been pointed out that directly implementing indices, which work for serial structures include drawbacks that render them useless for parallel manipulators. Starting from the singularity analysis of the parallel manipulators [4], where Merlet [3] found that the parallel UPU manipulator had previously undefined singularities because the end-effector was not regarded as a 6-DOF mechanism.

Although multiple serial manipulator indices like isotropy or the global conditioning number have been disregarded [3], due to being deemed unfit or computationally heavy, some indices have potential. Indices regarding dexterity, like manipulability, pointed out by Merlet [3], who used the Euclidean and infinity norm to map the errors and find relations between joint errors, thus laying a foundation for future research on the topic. He also mentioned the condition number to quantify manipulability to be used to assess the accuracy of robots, but also deemed one major flaw in the index. Similar to manipulability, it can only view translational and orientational error separately, thus movements involving both cannot be directly estimated. To overcome this, a workaround is proposed via normalization of the condition number, which is used in present papers as well [29].

Cardou et al. [22] were the first to develop indices for systems with a nonhomogeneous Jacobian matrix. The work is based on an experiment which is conducted to find compatible joint displacements to reach certain poses within the workspace. Multiple norms are tested and indices for each norm are found by using a geometrical constraint to bound the errors and then map the results via an objective function using the same norm. By doing so, compliance for redundantly actuated manipulators can be found and measures for maximal disposition can be shown with a clear physical meaning. Saadatzi et al. [22] followed this work by differentiating the norms of the constraint and objective function and postulated that using the ∞ - and 2-norm, respectively, is the most meaningful index for kinematic sensitivities since it accounts for changes in the coordinates.

Binaud et al. [24] uses Denavit-Hartenberg parameters and screw theory to allow the parameterization of joints in manipulators. By doing so, each joint has its own reference frame and the effect from one joint to another can be described using screws, this includes errors of

aforementioned joints. Thus, finding the index comes down to solving a relatively simple optimization problem. Also, by using this method, one is able to find maximum pose errors for moving-platforms even if the joints in the system may be axisymmetrical. In addition, while analysing the results of numerical examples, it is also noted that parallel manipulators perform significantly better in regard of overall displacements than serial mechanisms since joint displacements cancel each other out.

As can be seen from recent work by Lian et al. [28], new features for kinematic sensitivity indices have been developed as parameter sensitivity towards linear or overall stiffness performance is found. This addition has a lot of potential in today's world, because the complexity of manipulators along with the number of parameters keeps increasing, thus a method to sort out meaningful parameters according to performance set by designers is crucial. Also it is visible from [29] that artificial intelligence (AI) is being implemented to overcome some of the drawbacks like the difficult process of normalization which allows to assess the overall stiffness performance of a manipulator within the workspace. In addition, AI allows creating optimal designs using dimensional synthesis which negates the possibility of having singularities within the workspace.

Overall, kinematic sensitivity or accuracy assessment for parallel manipulators is seeing gradual improvement. Although a global sensitivity index has not been developed to compare the performance of different manipulators to each other, new features have been implemented through which multiple deficits have been overcome.

5.1 Future work

Taking the work of Lian et al. [26] as an example, there are some points which could be implemented to further improve the optimization, namely:

- Evaluating the parameter sensitivity via RSNC or RSPC and seeing which way the parameters affect performance, it might give new insights towards improving the selection of main parameters from subordinate ones.
- Considering elastic deformation of joints besides the IR joint. In the current paper FEA software is only used on IR joints to view the effect of elastic deformation towards performance.
- Viewing angular stiffness performance in addition to linear and overall would allow more accurate classification of parameters.

6 Summary

The goal of the thesis was to conduct a research on kinetostatic performance indices for parallel manipulators. It is done through an analysis on the developments in the field and a more detailed insight on a recent article posted on the subject. Limitations of the indices and proposals for future improvements are also included.

Firstly, an overview of robots in the industry is presented. The differences between parallel and serial manipulator architecture and performance originating from this, are briefly discussed. The usage areas of parallel manipulators are mentioned. In addition, because of the complex structure of parallel manipulators, the need for new indices is validated.

The literature review introduces the development process of the indices and provides a brief summary of the articles describing the process. Drawbacks of the proposed indices are brought out and the reasoning behind each improvement is illustrated via figures and equations.

In the recent work paragraph, a thorough analysis on a topical article about the development of a parameter sensitivity index through a complex five-degree-of-freedom manipulator using kinematic sensitivity as performance is presented. Parameters are pointed out along with the schematic of the structure and the calculation of the stiffness performance.

Lastly, a summary along with an analysis of the indices discussed throughout the thesis is carried out. The added value of each index is brought out along with shortcomings. Pointers for improving current indices are given at the end of the thesis.

7 Kokkuvõte

Antud lõputöö eesmärk oli läbi viia uurimus paralleelmanipulaatorite kinetostaatiliste jõudlusindeksite teemal. Sihid saavutatakse läbi valdkonnas esitatud teadustööde ja artiklite analüüsi ja ülevaate andmisega. Samuti esitatakse detailsem läbilõige hiljuti valminud artiklist toomaks välja hetkel kasutuses olevad indeksid. Lisatud on indeksite puudujäägid ning nõuanded tulevaseks arendustööks.

Esmalt antakse ülevaade robotite üleüldisest käekäigust tööstuses. Kirjeldatakse lühidalt erinevuseid paralleel- ja seriaalmanipulaatorite arhitektuuris ning sellest tulenevatest eripäradest. Tuuakse välja paralleelmehhanismide kasutusala ning nende ehitusest tulenevast vajadusest uute indeksite järgi.

Kirjandusliku ülevaate peatükis tutvustatakse indeksite arendusprotsessi ning pakutakse kokkuvõtte antud valdkonna teadusartiklitest. Tuuakse esile puudujäägid esitatud indeksitest ning tõendusmaterjal arendustööde paikapanevusest illustreeritakse erinevate jooniste ning võrrandite abil.

Neljandas peatükis sooritatakse põhjalik analüüs päevakohasest teadustööst, mille käigus arendati parameetrite tundlikkuse indeks keerukas viie vabadusastmega manipulaatori põhjal. Antud indeks võimaldab hinnata parameetrite mõju inseneride poolt sätestatud jõudlusele. Parameetrid tuuakse välja koos roboti skemaatilise struktuuriga samuti näidatakse jõudluse hindamiseks vajalike maatriksite arvutuskäiku.

Lõpetuseks analüüsitakse töö käigus välja toodud indeksite eripärad. Iga indeksi lisaväärtus koos puudujääkidega tuuakse esile ning punktid tulevaseks arenduseks tuuakse välja töö lõpuosas.

8 Acknowledgements

I would like to thank my supervisors Gholamreza Anbarjafari and Morteza Daneshmand for their support, providing me with the materials and giving me possibilities to improve myself and also for not giving up on me and helping me finalize my studies.

I would also like to thank my family, especially my grandmother who gave me the final push towards finishing my Master's studies.

Finally, I would like to thank my girlfriend who has been strong and supportive throughout this complicated process.

9 References

- [1] International Federation of Robotics, “Robots and the Workplace of the Future,” *Positioning Paper*, p. 35, 2018.
- [2] P. M. G. Y. D. Patel, “Parallel Manipulators Applications - A Survey,” *Modern Mechanical Engineering*, pp. 57-64, 9 February 2012.
- [3] J.P.Merlet, “Jacobian, Manipulability, Condition Number, and Accuracy of Parallel Robots,” *Transactions of the ASME*, no. 128, pp. 199-206, 2006.
- [4] J. A. Clement Gosselin, “Singularity Analysis of Closed-Loop Kinematic Chains,” *IEEE Transactions on Robotics and Automation*, pp. 281-290, June 1990.
- [5] D. Z. Ilian Bonev, “The Mystery of the Singular SNU Translational Parallel Robot,” *ParalleMIC*, 12 June 2001. [Online]. Available: <http://www.parallemic.org/Reviews/Review004.html>. [Accessed 5 May 2019].
- [6] T.-H. L. Ming-June Tsai, “Kinematic sensitivity analysis of linkage with joint clearance based on transmission quality,” *Mechanism and Machine Theory*, no. 39, pp. 1189-1206, 2004.
- [7] H. J. D. S. E. Staffetti, “On the Invariance of Manipulability Indices,” *Advances in Robot Kinematics*, pp. 57-66, 2002.
- [8] R. P. P. Kenneth H. Pittens, “A Family of Stewart Platforms with Optimal Dexterity,” *Journal of Field Robotics*, vol. 4, no. 10, pp. 463-479, 1993.
- [9] P. R. S. K. S. A.B.K. Rao, “Workspace and Dexterity Analysis of Hexaslide Machine Tools,” in *Proceedings of the 2003 IEEE International Conference on Robotics & Automation*, Taipei, Taiwan, 2003.

- [10] T. R.S. Stoughton, "A Modified Stewart Platform Manipulator with Improved Dexterity," *IEEE Transactions on Robotics and Automation*, vol. 2, no. 9, pp. 166-173, 1993.
- [11] I. E.-U. P.A. Voglewede, "Measuring "closeness" to singularities for parallel manipulators," in *IEEE International Conference on Robotics and Automation*, New Orleans, LA, USA, 2004.
- [12] H. H. A. G. S. Bhattacharya, "On the Optimum Design of a Stewart Platform Type Parallel Manipulators," *Robotica*, vol. 2, no. 13, pp. 133-140, 1995.
- [13] P. W. J. M. D. Chablat, "Workspace Analysis of the Orthoglide Using Interval Analysis," *Advances in Robot Kinematics - Theory and Applications*, no. 5, pp. 397-406, 2007.
- [14] J. S. A. M. Hay, "The Optimal Synthesis of Parallel Manipulators for Desired Workspace," ARK, Caldes de Malavalla, 2002.
- [15] J.-G. K. S. Hong, "Manipulability Analysis of a Parallel Machine Tool: Application to Optimal Link Length Design," *Journal of Robotic Systems*, vol. 8, no. 17, pp. 403-415, 2000.
- [16] K.-S. Hong, "Kinematic Optimal Design of a New Parallel-Type Rolling Mill: Paramill," *Advanced Robotics*, vol. 9, no. 17, pp. 837-862, 2003.
- [17] T. M. e. al., "Mechanism Configuration Evaluation of a Linear-Actuated Parallel Mechanism Using Manipulability," in *IEEE International Conference on Robotics and Automation*, Washington, 2002.
- [18] C.-W. T. a. G. C. W. R. C. Stamper, "Optimization of a Three DOF Translational Platform for Well-Conditioned Workspace," in *IEEE International Conference on Robotics and Automation*, Albuquerque, 1997.
- [19] S. J. L.-W. Tsai, "Kinematics and Optimization of a Spatial 3-UPU Parallel Manipulator," *Journal of Mechanical Design*, vol. 4, no. 112, pp. 439-446, 2000.

- [20] J. K. E. Zanganeh, "Kinematic Isotropy and the Optimum Design of Parallel Manipulators," *International Journal of Robotics Research*, vol. 2, no. 16, pp. 185-197, 1997.
- [21] C. Gosselin, "Kinematic Analysis Optimization and Programming of Parallel Robotic Manipulators," Ph.D. thesis, McGill University, Montreal, 1998.
- [22] S. B. C. G. P. Cardou, "Kinematic-Sensitivity Indices for Dimensionally Nonhomogeneous Jacobian Matrices," *IEEE Transactions on Robotics*, vol. 46, no. 1, pp. 166-173, 2009.
- [23] A. S. F. L. Ros, "An ellipsoidal calculus based on propagation and fusion," *IEEE Transactions on Systems, Man and Cybernetics part B*, vol. 32, no. 4, pp. 430-442, 2002.
- [24] P. C. S. C. P. W. N. Binaud, "The Kinematic Sensitivity of Robotic Manipulators to Joint Clearances," in *ASME 2010 International Design Engineering Technical Conferences and Computers and Information in Engineering Conference*, 2010.
- [25] M. T. M. H. D. T. C. G. P. M.H. Saadatzi, "Geometric Analysis of the Kinematic Sensitivity of Planar Parallel Mechanisms," *Transactions of the Canadian Society for Mechanical Engineering*, vol. 35, no. 4, pp. 477-489, 2011.
- [26] T. Y. B. Lian, "Parameter Sensitivity Analysis of a 5-DoF Parallel Manipulator," *Robotics and Computer-Integrated Manufacturing*, no. 46, pp. 1-14, 2017.
- [27] H. W. B. L. Y. Q. P. W. Y. S. T. Sun, "Stiffness Modeling, Analysis and Evaluation of a 5 Degree of Freedom Hybrid Manipulator for Friction Stir Welding," *Journal of Mechanical Engineering Science*, pp. 1-16, 2016.
- [28] T. Y. S. Y. J. M. B.Lian, "Stiffness Analysis and Experiment of a Novel 5-DoF Parallel Kinematic Machine Considering Gravitational Effects," *International Journal of Machine Tools and Manufacture*, no. 95, pp. 82-96, 2015.
- [29] T. S. B. L. G. Y. H. Y. Song, "A Novel Five-Degree-of-Freedom Parallel Manipulator and its Kinematic Optimizat0n," *Journal of Mechanisms and Robotics*, vol. 6, no. 4, pp. 041008-1-041008-9, 2014.

- [30] H. T. D. Y.Y. Wang, "Stiffness modeling of the Tricept robot using the overall Jacobian matrix," *Journal of Mechanisms and Robotics*, vol. 1, 2009.
- [31] P. W. J.-P. M. D. Chablat, "A Comparative Study Between Two Three-DOF Parallel Kinematic Machines Using Kinetostatic Criteria and Interval Analysis", 11th World Congress on Theory of Machines and Mechanisms, Tianjin, 2004.
- [32] D. Eppstein, "Zonohedra and Zonotypes," *Mathematica in Education and Research*, vol. 4, no. 5, pp. 15-21, 1996.
- [33] Brilliant.org, "Hessian Matrix," 2019. [Online]. Available: <https://brilliant.org/wiki/hessian-matrix/>. [Accessed 19 May 2019].

10 Appendices

Table 2 – Accuracy assessment of response models for subsystem I [26].

Error (Accepted level)	Order	M_1	η_{lx_1}	η_{ly_1}	η_{lz_1}	η_1
RS (> 0.9)	linear	0.99868	0.55946	0.86912	0.83863	0
	quadratic	1	0.95688	0.96161	0.98759	0.91945
	cubic	1	0.01265	0.0354	0.08955	0.0101
RAAE (< 0.2)	linear	0.00774	0.15036	0.09107	0.1008	1.10848
	quadratic	3.5024×10^{-8}	0.01767	0.0195	0.01472	0.02048
	cubic	2.4765 $\times 10^{-8}$	0.00853	0.00858	0.00913	0.00836
RMAE (< 0.3)	linear	0.01497	0.30800	0.22248	0.23559	2.7669
	quadratic	1.1228×10^{-7}	0.26604	0.18656	0.12557	0.29081
	cubic	8.20041 $\times 10^{-8}$	0.98117	0.98648	0.97309	0.98843
RMSE (< 0.2)	linear	0.00919	0.17077	0.10615	0.11757	1.35566
	quadratic	4.6011×10^{-8}	0.02621	0.02704	0.02034	0.03094
	cubic	2.80174 $\times 10^{-8}$	0.06776	0.06813	0.06726	0.06824

Table 3 – Accuracy assessment of response models for subsystem II [26].

Error (Accepted level)	Order	M_2	η_{lx_2}	η_{ly_2}	η_{lz_2}	η_2
RS (> 0.9)	linear	0.99868	0.96876	0.96893	0.9661	0.98119
	quadratic	1	0.99556	0.99557	0.99564	0.99636
	cubic	1	0.99990	0.99990	0.99990	0.99987
RAAE (< 0.2)	linear	0.00834	0.04259	0.04250	0.03797	0.03513
	quadratic	1.58548 $\times 10^{-5}$	0.01056	0.01052	0.00998	0.00935
	cubic	528461 $\times 10^{-6}$	0.00168	0.00170	0.00181	0.00193
RMAE (< 0.3)	linear	0.02043	0.09129	0.09054	0.09290	0.08687
	quadratic	6.94572 $\times 10^{-5}$	0.03575	0.03577	0.0329	0.04388
	cubic	1.42586 $\times 10^{-5}$	0.00876	0.00875	0.00837	0.00675
RMSE (< 0.2)	linear	0.01035	0.04783	0.04767	0.04408	0.04216
	quadratic	2.11149 $\times 10^{-5}$	0.01314	0.1309	0.01219	0.01194
	cubic	6.46371 $\times 10^{-6}$	0.06776	0.06813	0.06726	0.06824

Table 4 – Dimensional parameters and workspace of T5 PKM [28]

Dimensional parameters (mm)					workspace			
b	a	b_0	h_0	d	$H(\text{mm})$	$R(\text{mm})$	$h(\text{mm})$	$\varphi_{max}(\text{°})^a$
400	167	136	111	167.5	1200	400	300	40

^a φ_{max} is the maximum rotational angle of T5 PKM about x or y-axis

Table 5 – Lead screw parameters and compliance of R joints [28]

Lead screw		Linear Compliance			Angular Compliance		
Parameters		$(\mu\text{m}/\text{N}) \times 10^{-3}$			$(\text{rad}/(\text{N} \cdot \text{m})) \times 10^{-6}$		
$L_{sc}(\text{mm})$	$EA_{sc}(\text{MN})$	u'	v'	w'	u'	v'	w'
688	44.12	86.03	299.7	43.01	12.89	∞	16.52

Table 6 – Compliance coefficients of UPS limbs (unit: $(\mu\text{m}/\text{N}) \times 10^{-3}$) [28]

$c_{s,1}$	$c_{s,2}$	$c_{s,3,gr}^a$	$c_{s,3,q5}^b$	$c_{a,i,2}$	$c_{a,i,3}$	$c_{a,i,5}$	$c_{a,i,6}$	$c_{h,in}$	$c_{h,out}$
37.520	90.907	12.518	25.980	12.831	10.571	2.500	3.770	5.072	4.055

^a $c_{s,3,gr}$ is linear compliance of part 3 of S joints from j^{th} UPS limb ($j = 1,2,3,4$)

^b $c_{s,3,q5}$ is linear compliance of part 3 of S joints from 5th UPS limb

Table 7 – Lead screw parameters and compliance of R joints [28]

Lead screw		Linear Compliance			Angular Compliance		
Parameters		$(\mu\text{m}/\text{N}) \times 10^{-3}$			$(\text{rad}/(\text{N} \cdot \text{m})) \times 10^{-6}$		
$L_{sc}(\text{mm})$	$EA_{sc}(\text{MN})$	u'	v'	w'	u'	v'	w'
688	44.12	86.03	299.7	43.01	12.89	∞	16.52

Table 8 – Compliance coefficients of UP limb [28]

$c_{u,in}$	$c_{v,in}$	$c_{w,in}$	$c_{u,out}$	$c_{v,out}$	$c_{w,out}$	$EI(\text{MN})$	$GI_t(\text{MN})$
0.787	34.843	1.190	4.310	4.762	0.041	2.852	1.103

Table 9 – Component compliance coefficients of closed-loop I in substructure II[28]

	Linear Compliance			Angular Compliance		
	$(\mu\text{m}/\text{N}) \times 10^{-3}$			$(\text{rad}/(\text{N} \cdot \text{m})) \times 10^{-6}$		
	\bar{u}_1	\bar{v}_1	\bar{w}_1	\bar{u}_1	\bar{v}_1	\bar{w}_1
${}^2\bar{\mathcal{C}}_{ac,1}$	1.076	0.357	1.213	0.231	∞	0.0117
${}^2\bar{\mathcal{C}}_{1,1}$	48.408	965.38	0.102	0.176	∞	0.0102
${}^2\bar{\mathcal{C}}_{2,1}$	0.465	1.938	2.009	∞	∞	0.0150
${}^2\bar{\mathcal{C}}_{3,1} ({}^2\bar{\mathcal{C}}_{4,1})$	∞	97.176	1.531	∞	∞	0.00172
${}^2\bar{\mathcal{C}}_{5,1}$	0.0612	0.0642	0.1184	∞	∞	0.00473
${}^2\bar{\mathcal{C}}_{E_3E_4}$	23.634	87.346	3.213	0.0274	∞	0.316

Table 10 – Component compliance coefficients of closed-loop II in substructure II[28]

	Linear Compliance			Angular Compliance		
	$(\mu\text{m}/\text{N}) \times 10^{-3}$			$(\text{rad}/(\text{N} \cdot \text{m})) \times 10^{-6}$		
	\bar{u}_2	\bar{v}_2	\bar{w}_2	\bar{u}_2	\bar{v}_2	\bar{w}_2
${}^2\bar{\mathcal{C}}_{ac,2}$	0.357	1.076	1.213	∞	0.231	0.0117
${}^2\bar{\mathcal{C}}_{1,2} ({}^2\bar{\mathcal{C}}_{2,2})$	52.388	∞	18.834	∞	0.0612	0.0316
${}^2\bar{\mathcal{C}}_{3,2} ({}^2\bar{\mathcal{C}}_{4,2})$	6.929	∞	∞	∞	0.0642	0.0917
${}^2\bar{\mathcal{C}}_{5,2}$	0.126	∞	0.104	∞	0.1184	0.0028
${}^2\bar{\mathcal{C}}_{F_3F_4}$	1.336	9.735	0.721	0.0132	0.0357	0.0142

Table 11 – Mass and centre of mass of components in substructure I[28]

${}^1m_{L_1}(\text{kg})$	${}^1m_{L_2}(\text{kg})$	${}^1m_{IR_{ja}}(\text{kg})$	$\rho A_C(\text{kg}/\text{m})$	${}^1m_P(\text{kg})$	${}^1l_1(\text{mm})$	${}^1l_2(\text{mm})$	${}^1l_P(\text{mm})$
14.501	7.473	3.434	37.758	20.142	198.65	405.27	25.61

Table 12 – Mass and centre of mass of components in substructure II [28][28]

	Mass(kg)	Coordinate of Central Point (mm)		
		\bar{u}_2	\bar{v}_i	\bar{w}_2
link E_1E_2	6.390	0.95	-0.8	-209.83
link $E_1E_4 (E_2E_3)$	0.607	-60(60)	0	-96.46
link E_3E_4	3.582	0	0	26.95
link F_1F_2	2.839	-4.07	0	-173.89
link $F_1F_4(F_2F_3)$	0.861	0	65(-65)	-98.11
link F_3F_4	3.893	0	0	25.95
U joint in closed-loop I	0.133	-60(60)	0	12.98
U joint in closed-loop II	0.133	0	65(-65)	12.98

Table 13 – Global parameter sensitivity of performance reliability in subsystem I [26]

	k_u	D_{op}	d_{op}	d_s	D_{ip}	d_{ip}	k_s	D_{ir_1}	d_{ir_1}	d_{ir_2}
ε_{M_1}	0.0000	1.0477	0.6280	0.0154	0.9655	0.4847	0.0000	0.1272	0.0799	0.0191
ε_{M_1}	0.0006	0.0056	0.0126	0.1824	0.0525	0.0627	0.2176	0.0559	0.0500	0.3225
ε_{M_1}	0.0016	0.0326	0.0479	0.2169	0.0193	0.0795	1.4142	0.0301	0.0126	0.0781
ε_{M_1}	0.0014	0.0269	0.0353	0.1465	0.0186	0.0646	1.2048	0.2352	0.0668	0.7934
ε_{M_1}	0.0026	0.1086	0.0219	1.1074	0.0115	0.1927	0.5806	0.0989	0.3254	1.0115
	k_U	k_V	D_{ct}	d_{ct}	D_{op_5}	d_{op_5}	d_{s_5}	D_{ip_5}	d_{ip_5}	k_{s_5}
ε_{M_1}	0.0000	0.0000	1.4142	1.0368	0.2094	0.1618	0.0038	0.1958	0.1352	0.0000
ε_{M_1}	0.0174	0.0029	0.0197	0.0157	0.0155	0.0474	0.2377	0.0265	0.1123	1.4142
ε_{M_1}	0.0002	0.0009	0.0117	0.0040	0.0210	0.0502	0.2510	0.0110	0.1046	0.0509
ε_{M_1}	0.0083	0.0037	0.0121	0.0039	0.0265	0.0527	0.1915	0.0137	0.0961	1.4142
ε_{M_1}	0.0120	0.0043	0.1881	0.1636	0.1239	0.2179	0.8177	0.1754	0.4198	0.2546

Table 14 – Global parameter sensitivity of performance reliability in subsystem II [26]

	d_{ir_2}	a_{11}	b_{11}	a_{21}	a_{31}	a_{41}	b_{21}	a_{51}	b_{31}	c_{11}
ε_{M_1}	0.0000	1.0000	0.6372	0.8247	0.5000	0.4267	0.3342	0.4963	0.3575	0.6471
ε_{M_1}	0.0012	0.0003	0.0002	0.0000	0.0000	0.0000	0.0000	0.0001	0.0000	1.4142
ε_{M_1}	0.0011	0.0003	0.0002	0.0000	0.0000	0.0000	0.0000	0.0001	0.0000	1.4142
ε_{M_1}	0.0011	0.0002	0.0001	0.0008	0.0000	0.0000	0.0000	0.0002	0.0001	1.0013
ε_{M_1}	0.0059	0.0100	0.0007	0.0008	0.0001	0.0001	0.0001	0.0213	0.0053	0.0960
	c_{21}	c_{31}	c_{41}	c_{51}	a_{12}	b_{12}	a_{22}	a_{32}	b_{22}	
ε_{M_1}	0.0717	1.0027	0.0000	0.0000	0.5038	0.7333	0.6654	0.6834	0.3515	
ε_{M_1}	0.0099	0.6471	0.0000	0.0000	0.0001	0.0002	0.0007	0.0000	0.0001	
ε_{M_1}	0.0101	0.6315	0.0000	0.0000	0.0000	0.0004	0.0006	0.0001	0.0000	
ε_{M_1}	0.1190	1.3722	0.0000	0.0004	0.0006	0.0001	0.0000	0.0000	0.0961	
ε_{M_1}	0.5170	1.4142	0.0001	0.0005	0.0008	0.0012	0.0002	0.0000	0.0000	

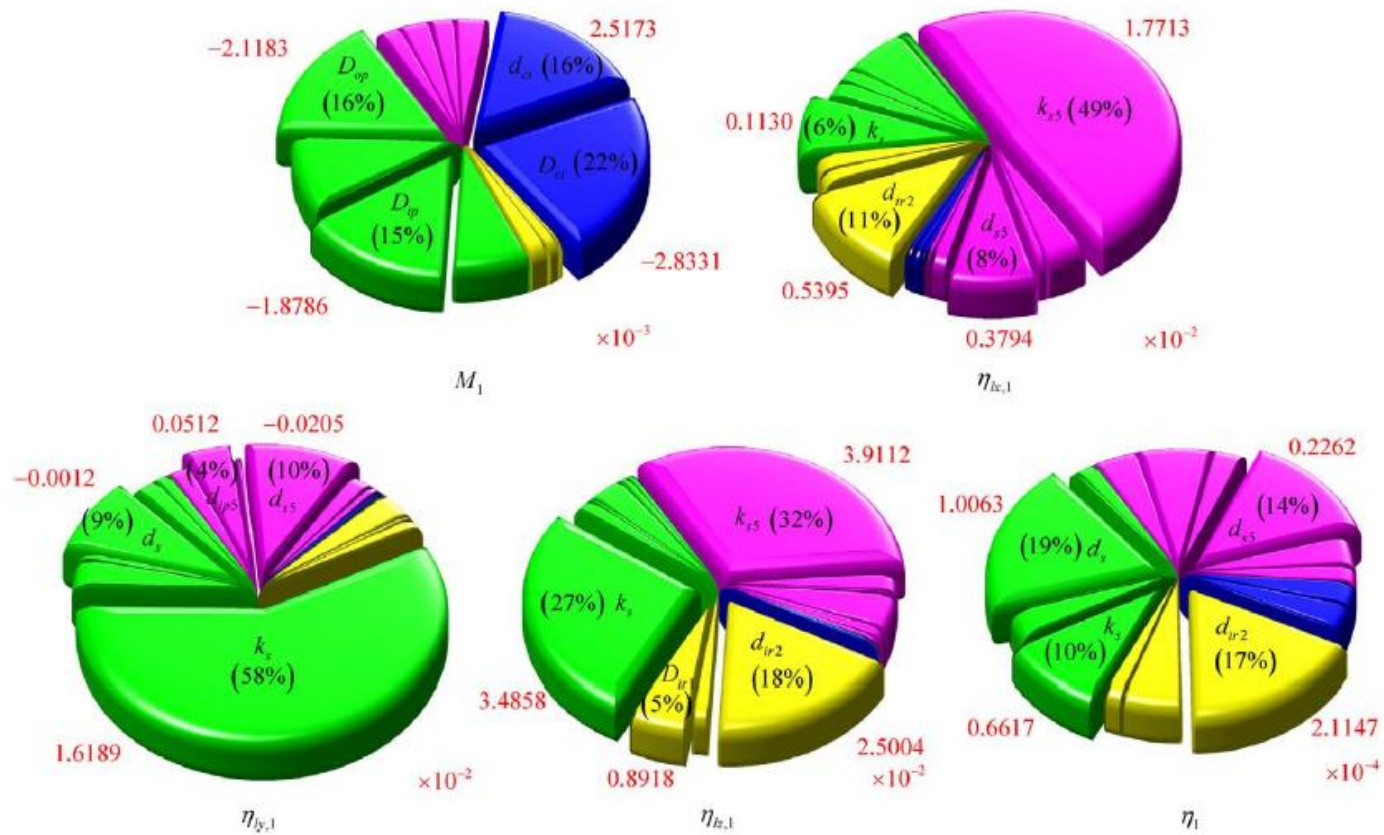


Figure 20 – Proportions of parameter impacts to performance reliability of subsystem I (green: 1st to 4th UPS limbs, yellow: IR joints, blue: UP limb, pink: 5th UPS limb, red numbers indicating corresponding reliability sensitivity to parameter mean values) [26]

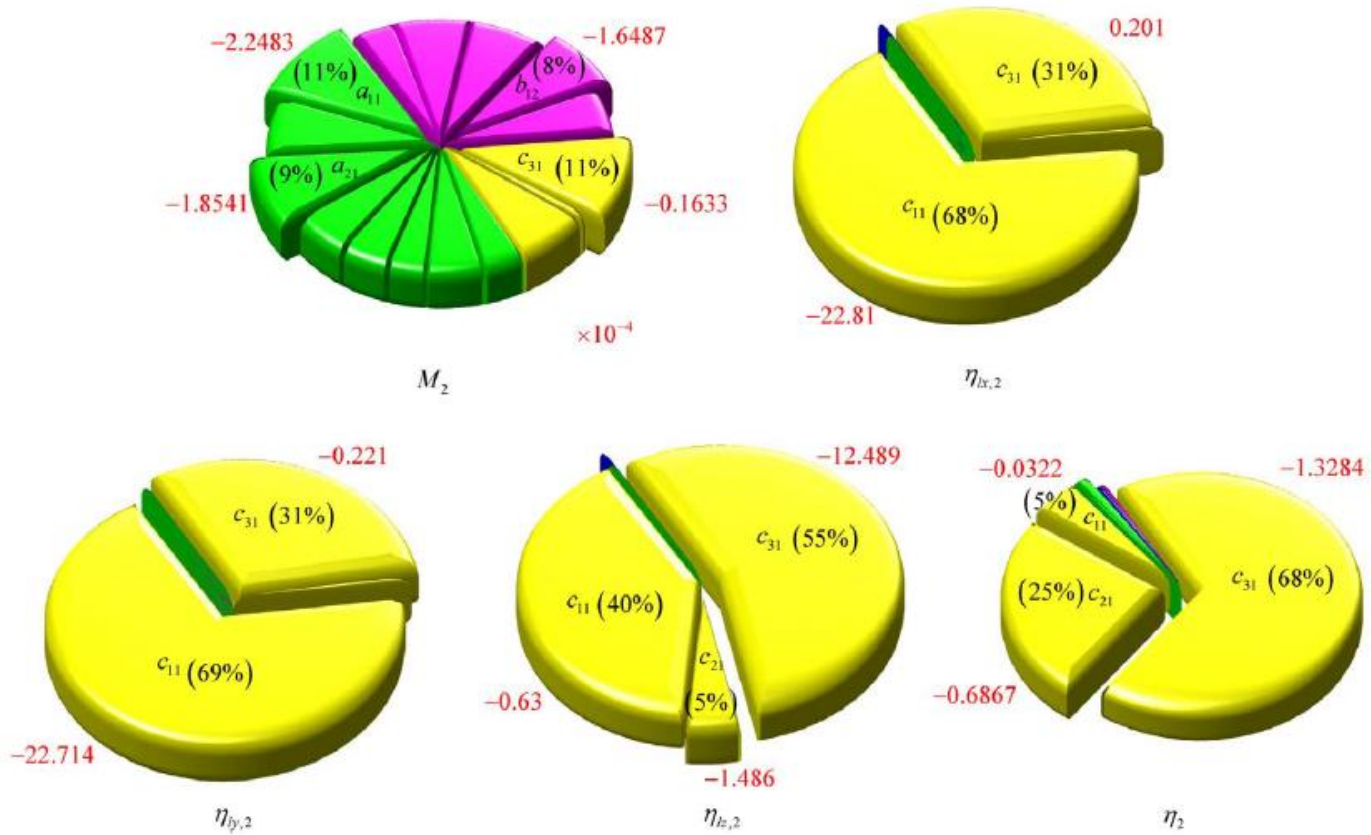


Figure 21 – Proportions of parameter impacts to performance reliability of subsystem II (green: 1st to 4th UPS limbs, yellow: IR joints, blue: UP limb, pink: 5th UPS limb red numbers indicating corresponding reliability sensitivity to parameter mean values) [26]

Non-exclusive licence to reproduce thesis and make thesis public

I, Ott Sellis,

1. herewith grant the University of Tartu a free permit (non-exclusive licence) to

reproduce, for the purpose of preservation, including for adding to the DSpace digital archives until the expiry of the term of copyright,

Investigation and Comparison of Kinetostatic Performance Indices for Parallel Mechanisms,

supervised by Assoc. Prof. Gholamreza Anbarjafari and Morteza Daneshmand

2. I grant the University of Tartu a permit to make the work specified in p. 1 available to the public via the web environment of the University of Tartu, including via the DSpace digital archives, under the Creative Commons licence CC BY NC ND 3.0, which allows, by giving appropriate credit to the author, to reproduce, distribute the work and communicate it to the public, and prohibits the creation of derivative works and any commercial use of the work until the expiry of the term of copyright.
3. I am aware of the fact that the author retains the rights specified in p. 1 and 2.
4. I certify that granting the non-exclusive licence does not infringe other persons' intellectual property rights or rights arising from the personal data protection legislation.

Ott Sellis

20/05/2019